

University of Windsor

## Scholarship at UWindso

---

Electronic Theses and Dissertations

Theses, Dissertations, and Major Papers

---

1992

### A study of vortex diodes at low Reynolds number.

Jojo P. Mathai  
*University of Windsor*

Follow this and additional works at: <https://scholar.uwindsor.ca/etd>

---

#### Recommended Citation

Mathai, Jojo P., "A study of vortex diodes at low Reynolds number." (1992). *Electronic Theses and Dissertations*. 826.

<https://scholar.uwindsor.ca/etd/826>

This online database contains the full-text of PhD dissertations and Masters' theses of University of Windsor students from 1954 forward. These documents are made available for personal study and research purposes only, in accordance with the Canadian Copyright Act and the Creative Commons license—CC BY-NC-ND (Attribution, Non-Commercial, No Derivative Works). Under this license, works must always be attributed to the copyright holder (original author), cannot be used for any commercial purposes, and may not be altered. Any other use would require the permission of the copyright holder. Students may inquire about withdrawing their dissertation and/or thesis from this database. For additional inquiries, please contact the repository administrator via email ([scholarship@uwindsor.ca](mailto:scholarship@uwindsor.ca)) or by telephone at 519-253-3000ext. 3208.



National Library  
of Canada

Acquisitions and  
Bibliographic Services Branch

395 Wellington Street  
Ottawa, Ontario  
K1A 0N4

Bibliothèque nationale  
du Canada

Direction des acquisitions et  
des services bibliographiques

395, rue Wellington  
Ottawa (Ontario)  
K1A 0N4

*Your file - Votre référence*

*Our file - Notre référence*

## NOTICE

The quality of this microform is heavily dependent upon the quality of the original thesis submitted for microfilming. Every effort has been made to ensure the highest quality of reproduction possible.

If pages are missing, contact the university which granted the degree.

Some pages may have indistinct print especially if the original pages were typed with a poor typewriter ribbon or if the university sent us an inferior photocopy.

Reproduction in full or in part of this microform is governed by the Canadian Copyright Act, R.S.C. 1970, c. C-30, and subsequent amendments.

## AVIS

La qualité de cette microforme dépend grandement de la qualité de la thèse soumise au microfilmage. Nous avons tout fait pour assurer une qualité supérieure de reproduction.

S'il manque des pages, veuillez communiquer avec l'université qui a conféré le grade.

La qualité d'impression de certaines pages peut laisser à désirer, surtout si les pages originales ont été dactylographiées à l'aide d'un ruban usé ou si l'université nous a fait parvenir une photocopie de qualité inférieure.

La reproduction, même partielle, de cette microforme est soumise à la Loi canadienne sur le droit d'auteur, SRC 1970, c. C-30, et ses amendements subséquents.

Canada

**A STUDY OF VORTEX DIODES AT LOW REYNOLDS NUMBER**

by

**Jojo P. Mathai**

**A Thesis**

**Submitted to the Faculty of Graduate Studies and Research  
through the Department of Mechanical Engineering in  
Partial Fulfilment of the Requirements for the  
Degree of Master of Applied Science at the  
University of Windsor**

**Windsor, Ontario, Canada  
1992**



National Library  
of Canada

Acquisitions and  
Bibliographic Services Branch

395 Wellington Street  
Ottawa, Ontario  
K1A 0N4

Bibliothèque nationale  
du Canada

Direction des acquisitions et  
des services bibliographiques

395, rue Wellington  
Ottawa (Ontario)  
K1A 0N4

*Your file*  *Votre référence*

*Our file*  *Notre référence*

**The author has granted an irrevocable non-exclusive licence allowing the National Library of Canada to reproduce, loan, distribute or sell copies of his/her thesis by any means and in any form or format, making this thesis available to interested persons.**

**L'auteur a accordé une licence irrévocable et non exclusive permettant à la Bibliothèque nationale du Canada de reproduire, prêter, distribuer ou vendre des copies de sa thèse de quelque manière et sous quelque forme que ce soit pour mettre des exemplaires de cette thèse à la disposition des personnes intéressées.**

**The author retains ownership of the copyright in his/her thesis. Neither the thesis nor substantial extracts from it may be printed or otherwise reproduced without his/her permission.**

**L'auteur conserve la propriété du droit d'auteur qui protège sa thèse. Ni la thèse ni des extraits substantiels de celle-ci ne doivent être imprimés ou autrement reproduits sans son autorisation.**

ISBN 0-315-78672-0

**Canada**

© Jojo P. Mathai 1992

## **ABSTRACT**

Knowledge of the flow characteristics of geometrically similar vortex diodes of different dimensions is essential in establishing the possible application of miniaturized vortex diodes in the medical field. The objective of this study is to find out whether Reynolds number and Euler's number are sufficient to describe the vortex diode performance and to experimentally verify the results obtained by finite element analysis.

The steady-state, incompressible, three-dimensional, confined flow of water through vortex diodes at low Reynolds numbers was numerically and experimentally investigated. Three geometrically similar Plexiglas vortex diodes were constructed and tested for flows at low Reynolds numbers. The pressure drop across each diode was measured for various flow rates. Static characteristics of the vortex diodes for both forward and reverse flows are presented.

The results indicate that in the Reynolds number range of  $200 < Re < 3000$  there is no noticeable scale effect on the static characteristics of the vortex diode. The Reynolds number is defined by the average axial velocity in the axial pipe and its diameter. The results also indicate that, due to the possible influence of viscous effects, the performance ratios are relatively small compared to those obtained at higher Reynolds numbers. There is also good agreement between the numerical and experimental results.

To my parents

## **ACKNOWLEDGEMENTS**

The author wishes to express his deep and sincere gratitude to Drs. K. Sridhar and G. W. Rankin for their excellent guidance, continuous support and infinite patience during the course of this study. The valuable suggestions of Dr. T. W. McDonald and Dr. A. W. Gryn are gratefully acknowledged.

Thanks are due to Dr. Gilles Delaire for his help in many areas. I also wish to thank Satya Kurada, Soumitra Basu and Vijayakanthan Damodaran for their encouragement and timely assistance.

Technical assistance rendered by Mr. R. Tattersall in constructing the test facility is gratefully acknowledged. Thanks go to Mr. M. Drouillard for his help in working with the Sun SPARCstation2™.

The study was financially supported by Natural Sciences and Engineering Research Council of Canada through Grant Numbers A-2190 and A-1403.



## TABLE OF CONTENTS

	Page	
ABSTRACT	iv	
DEDICATION	v	
ACKNOWLEDGEMENTS	vi	
LIST OF FIGURES	ix	
LIST OF TABLES	x	
NOMENCLATURE	xi	
CHAPTER I	INTRODUCTION	1
	1.1 Subject of Investigation	1
	1.2 Motivation	2
	1.3 Objectives	3
	1.4 Format of Presentation	4
CHAPTER II	LITERATURE SURVEY	5
	2.1 Fluidics	5
	2.1.1 Fluidic Devices	6
	2.2 Vortex Flow Theory	9
	2.3 Non-dimensional Variables and Characteristic Curves	12
CHAPTER III	EXPERIMENTAL INVESTIGATION	13
	3.1 Introduction	13
	3.2 Experimental Equipment	14
	3.2.1 General Test Facility	14
	3.2.2 Rotameter	15
	3.2.3 Manometer	15
	3.2.4 Vortex Diode	15
	3.3 Experimental Procedure	16
	3.4 Results and Discussion	17
CHAPTER IV	NUMERICAL STUDY	20
	4.1 Introduction	20
	4.2 NISA/3D-FLUID	21
	4.3 Finite Element Modelling	23
	4.3.1 Discretization	23
	4.3.2 Boundary Conditions	23

	4.3.3 Finite Element Equations	24
	4.3.4 Assembly and Solution	26
	4.3.5 Post Processing	27
	4.4 Results	27
	4.5 Discussion	28
CHAPTER V	SUMMARY OF CONCLUSIONS AND RECOMMENDATIONS	29
	5.1 Conclusions	29
	5.2 Recommendations	29
REFERENCES		31
FIGURES		35
TABLES		61
APPENDICES		
	A Uncertainty Analysis	64
	B Equipment Table	73
	C Rotameter Calibration	75
	D Experimental Data	81
VITA AUCTORIS		88

## LIST OF FIGURES

Figure	Title	Page
1.1	Reverse Flow	36
1.2	Forward Flow	37
2.1	Vortex Amplifier	38
2.2	Characteristic Curve (Zobel) Forward Flow	39
2.3	Characteristic Curve (Zobel) Reverse Flow	40
3.1	Schematic Diagram of Test Facility	41
3.2	Isometric View of Test Diode	42
3.3	Sectional A - A	43
3.4	Sectional B - B	44
3.5	Pressure Drop Vs. Flow Rate Forward Flow	45
3.6	Pressure Drop Vs. Flow Rate Reverse Flow	46
3.7	Characteristic Curve Forward Flow	47
3.8	Characteristic Curve Reverse Flow	48
3.9	Best-fit Curve Forward Flow	49
3.10	Best-fit Curve Reverse Flow	50
3.11	Performance Ratio Vs. Reynolds Number	51
4.1	NISA Fluid Flow Analysis Flow Chart	52
4.2	Finite Element Discretization of Vortex Chamber	53
4.3	Finite Element Discretization of Tangential Inlet	54
4.4	8-Noded Hexahedral Element	55
4.5	Pressure Drop Vs. Flow Rate Diode 1 Forward Flow	56
4.6	Pressure Drop Vs. Flow Rate Diode 1 Reverse Flow	57
4.7	Characteristic Curve Diode 1 Forward Flow	58
4.8	Characteristic Curve Diode 1 Reverse Flow	59
4.9	Performance Ratio Vs. Reynolds Number	60

## LIST OF TABLES

Table	Title	Page
3.1	Dimensions of Test Diodes	62
4.1	Element Description	63

## NOMENCLATURE

$C_v$	specific heat at constant volume, J/kg.K
$d$	axial pipe diameter, m
$D$	vortex chamber diameter, m
$Eu$	Euler number based on average velocity in axial pipe in equation 2.1
$f$	body force, N
$h$	chamber height, m
$K$	thermal conductivity, J/sec.m.K
$p$	pressure, Pa
$q_s$	heat source, J/sec.m <sup>2</sup>
$r$	radius, m
$R$	residual resulting from the use of approximations in equation 4.11
$Re$	Reynolds number based on average velocity in the axial pipe in equation 2.2
$t$	time, sec
$T$	temperature, K
$u$	velocity component, m/sec
$v$	tangential velocity, m/sec
$V$	average velocity in axial pipe, m/sec
$w$	weighting function in equation 4.12
$x$	distance, m
$[k],[K]$	stiffness matrices

$[m],[M]$	mass matrices
$\{\dot{u}\}$	gradient of $u$ with respect to time vector
$\{u\}$	nodal velocity vector
$\{s\}$	source vector

### Greek Symbols

$\theta$	inclination of manometer, degrees
$\lambda$	second viscosity coefficient
$\mu$	dynamic viscosity coefficient, kg/m.sec
$\rho$	density, kg/m <sup>3</sup>
$\Phi$	dissipation term
$\Omega$	element domain

### Subscripts

$a$	axial
$i,j,k$	coordinate directions
$i,o$	inlet and outlet
$t$	tangential

## CHAPTER I

### INTRODUCTION

#### 1.1 Subject of Investigation

This study deals with the steady-state, incompressible, three-dimensional confined flow through vortex diodes. The study and development of vortex diodes and other fluidic devices is known as Fluidics.

Fluidics is the technology that exploits the hydrodynamic properties of fluids to eliminate or complement mechanical parts of equipment. This technology deals with the art of moving and controlling flows of fluids using controllers, no-moving part valves and pumps. The term Fluierics is used for the specific study of non-moving part devices, while Fluidics is a somewhat broader definition which includes peripheral equipment such as transducers and accelerometers. Fluidics technology became first known in the early 1960s through the work done at the Harry Diamond Laboratories in Washington, D.C. [W2]. The objective of the work was to develop fluidic logic and control techniques as alternatives to electrical control systems principally for military application. This work combined a knowledge of control systems technology with that of fluid mechanics. The technology of fluidics is based on the application of a number of fluid flow phenomena, in particular those of entrainment, vortex flow and wall attachment, which could be used singly, or in combination to pump, direct fluid flows and control fluid pressure. Devices based on the above technology are known as

Fluidic devices. Fluidic devices, since they have no moving parts, infer high reliability and long life.

The vortex diode was first well characterized by Zobel [F1]. Vortex diodes are passive elements which offer a) low resistance to flow in one direction and b) high resistance when flow is reversed. The vortex diode consists of a short cylindrical chamber with two ports. One port is tangential to the chamber and the other along the axis. The operation of the diode can be understood from the following discussion. In the reverse flow direction, the fluid enters the diode tangentially and forms a vortex as shown in Figure 1.1. Due to the formation of the vortex, centrifugal forces come into effect, which tend to push the flow toward the outer wall, away from the central axial exit port. The pressure drop across the diode is thus the sum of the resistance due to the adverse pressure gradient due to the centrifugal effect and the frictional pressure drop. In the low-resistance direction the fluid enters the chamber through the axial port without forming a vortex and loses a small amount of pressure (Figure 1.2).

## **1.2 Motivation**

The characteristics of the vortex diode have made it very attractive for various industrial applications. In the nuclear industry, it has been used in fluidic pumping systems for handling highly radioactive fluids and in the coolant system of gas cooled reactors to prevent rapid depressurization in the event of a pipe fracture. In the chemical industry it has been used for highly corrosive and other fluids that



are difficult to handle. Vortex diodes can be used in both compressible and incompressible flow situations. Traditionally, the vortex diode was studied in connection with flow at high Reynolds numbers. This may be attributed to the fact that practical applications of diodes have been in areas of high flow rate.

The analysis of the flow through a vortex diode based on inviscid theory does not yield good results at low Reynolds numbers because, at low Reynolds numbers, the viscous effects on the flow are considerable and cannot be neglected. The analytical investigation taking into consideration the viscous and boundary layer effect is complicated and hence with the development of numerical techniques for solving the flow equations, it was decided to model the vortex diode and investigate the flow numerically.

The motivation for the present study was to determine the performance of the vortex diodes when they are miniaturized and used at low Reynolds numbers with potential application in the medical field. In the medical field the application of a miniaturized vortex diode was proposed to function as a shunt in draining the cerebro-spinal fluid from the head to the abdominal cavity in persons with brain hemorrhage. The presence of any geometrical scale effects was investigated by studying the static characteristics of three geometrically similar vortex diodes. The three-dimensional flow simulation package NISA/3D-FLUID™ package was used to model and analyze the flow through the vortex diodes at low Reynolds numbers. The package is based on the finite element method and was chosen since it can handle complex geometries more conveniently than the finite difference scheme.

### **1.3 Objectives**

The overall objectives of the present study were:

- a) To experimentally determine the performance of the vortex diodes at low Reynolds numbers.
- b) To obtain the static characteristics of the vortex diode at low Reynolds numbers using numerical techniques for solving the flow equations.
- c) To investigate the influence of any scale effect on the performance of the vortex diode.
- d) To compare the numerical results obtained using NISA/3D-FLUID™ with the experimental results.

### **1.4 Format of Presentation**

In the second chapter, the literature survey reviews the development of the Fluidics technology and some applications of vortex devices. Some of the performance parameters are also defined.

The details of the experimental set-up, procedure and results are described in chapter three. Chapter four deals with the numerical study and the results obtained are discussed. The conclusions and recommendations are provided in chapter five. The appendices contain the uncertainty analysis, equipment table, rotameter calibration curves and tables of data.

## **CHAPTER II**

### **LITERATURE SURVEY**

This chapter includes a survey of the literature pertaining to the study of vortex diodes. The material is presented in the following sections:

- a) Fluidics
- b) Vortex Flow Theory
- c) Non-dimensional Variables and Characteristic Curves.

#### **2.1 Fluidics**

The concept of no-moving part fluid control devices was first announced by the Harry Diamond Laboratories in 1960 under the name of Pure Fluidic Devices. Fluierics and Fluidics technology developed from this field.

Fluidics technology has objectives similar to those of electronics, but utilizes the fluidic dynamic phenomena instead of electron ballistics and field effects. Fluidics can be divided into two main areas of study: Signal Control Fluidics and Power Fluidics. In Signal Control Fluidics, the devices are usually operated with air and are used to perform mathematical functions to control some kind of actuators which in turn control the process fluid.

In Power Fluidics, the fluid energy present in the process fluid itself is exploited in no-moving part devices. These devices can be used in place of conventional mechanical equipment such as pumps and valves, to provide in an improvement

in the reliability of the system. In Power Fluidics two signals are important: flow and pressure. A wide range of fluid dynamic phenomena have been employed in Power Fluidics to utilize the energy inherent in the fluid. Some of the phenomena used are the fluid vortex, the directed jet and the Coanda effect. Elements or devices which utilize the above phenomena are called fluidic devices.

### **2.1.1 Fluidic Devices**

Fluidic devices are control elements which operate without being dependent on manual handling and extraneous energy and perform complicated control operations without using moving parts.

Fluidic devices meet the following conditions [P1]:

- a) The element should not have moving parts.
- b) The element should be controllable.
- c) The output rates should have dimensions suitable for practical hydraulic engineering.
- d) Nozzles and pipes should be big enough to prevent plugging by soiling.
- e) The shape of the element should be simple in order to reduce the production cost.

The main advantages of fluidic devices are their high reliability, operation in extreme conditions of temperature, safe operation in explosive atmospheres, resistance to shock and vibration, and freedom from interference from radiation in radioactive environments. In addition, the costs of the elements are low [E2].

Kirshner [K1] classified fluidic devices on the basis of the underlying fluid dynamic phenomena affecting their operation. Devices which utilize the vortex flow phenomenon for its operation are called vortex devices. The important types of vortex devices are the vortex rate sensor, vortex diode and the vortex amplifier.

### **Vortex Amplifier**

The vortex amplifier (also known as vortex triode) is a fluidic device which has the function of modulating the total power output from a pipe supplying fluid. It consists of a thin cylindrical chamber with three ports: a radial supply port which supplies the main portion of the flow to the amplifier, a tangential control port which supplies the flow which drives the vortex and an axial exit port through which all flow leaves the amplifier (Figure 2.1).

The vortex amplifier has been used as, an hydraulic servovalve stage, a thrust vector controller, a rate gyro, a pressure controller and a controller in the ventilation system of radioactive enclosures.

### **Vortex Diode**

The use of vortex effects in fluidic devices was first described by D. Thoma [B2]. The vortex diode is essentially a vortex amplifier without the radial supply port. Vortex diodes are passive elements which offer different resistances to the fluid flow depending upon which direction it flows through the device. Zobel improved the design of vortex diodes and his optimum design is regarded as the best available compromise between good performance and ease of manufacture.

The typical flow characteristics of the Zobel diode are shown in Figure 2.2 and Figure 2.3 [P1].

The development of other types of vortex diode have been reported by Sidhu et al. [S1]. One design, referred to as a Catherine wheel diode, has multiple tangential ports, a thin radial diffusing chamber and either one or two axial ports. Thin chamber diodes are generally more difficult to manufacture and more prone to blockage. For certain flow conditions the Catherine wheel diode is claimed to have a performance superior to that of the Zobel diode.

George et al. [G1] experimentally investigated the flow patterns inside high performance vortex diodes and developed a predictive technique to deduce the distribution of tangential velocity using the static pressure distribution inside the vortex chamber. Jacobs and Baker [J1] studied the transient response of vortex diodes. They found that the transient response can be correlated with the time taken for the initial volume of stationary fluid within the vortex chamber to be displaced by the incoming fluid. Wormley [W2] presented a review on the static and dynamic design techniques for vortex diodes and triodes.

Besides vortex diodes, other types of fluidic diodes have been developed, namely the scroll diode, the cascade diode and the momentum fluidic diode. Baker [B1] reported a comparative study of the different types of diodes and none of the other diodes could match the overall performance of the vortex diode.

McGuigan et al. [M1] developed a method of replacing the mechanical valves in reciprocating pumps by a bridge-configuration of vortex diodes. Priestman et al. [P1] point out the problem of cavitation in vortex diodes used in fluidic pumping

systems. Syred and Roberts [S2] reported on the application of vortex diodes to post accident heat removal systems in nuclear power plants.

The characteristics of the vortex diodes have made them very attractive to the nuclear industry where they are fitted at the entry to the reactor core to prevent rapid depressurisation of the reactor core in the event of a pipe failure. Beyond the nuclear industry they have found application in the chemical industry to handle highly corrosive and erosive fluids [E2].

## **2.2 Vortex Flow Theory**

Knowledge of vortex flow theory is important for the proper design and operation of cyclone dust separators, centrifugal burners, vortex devices and plasma-flame stabilization. The prediction of three dimensional velocity profiles as a function of the operating conditions and geometry of the vortex system is a major consideration in analysis and design. The complexity of vortex motion and the existence of secondary flows in the confining equipment have so far hindered the complete understanding of the detailed mechanics of the vortex flow. The non-linear character of the governing equations coupled with the complex boundary conditions make the mathematical solution of the confined vortex flow a formidable task [V1]. Many investigations have over-simplified the complexities of the flow and only a few analyses have considered the effect of geometrical parameters.

The operation and behaviour of a vortex diode can be understood better with a sound knowledge of confined vortex flow theory. Experimental and theoretical results of the study of the confined vortex flow agree in the following important

aspects [R1] :

- a) The confined vortex flow is three dimensional in nature.
- b) The tangential velocity component is predominant and the radial velocity component is very small in the entire vortex flow.
- c) An important radial flow toward the centre occurs in a region adjacent to the wall. Some workers also measured a substantial axial flow in the maximum tangential velocity component region.
- d) The axial velocity may show a reversal near the axis of the vortex chamber.
- e) The tangential velocity profile in the radial direction is composed mainly of two regions: a peripheral region of quasi-free vortex ( where  $v \cdot r = \text{constant}$  ) and a central part of quasi-forced vortex flow (  $v = \text{constant} \cdot r$  ).
- f) In a vortex flow, there may be a helical shaped dynamic axis of rotation.
- g) The angle of inlet flow may change the axial flow pattern, mainly near the walls of the vortex chamber.
- h) The static pressure is high near the walls confining the vortex flow and decreases drastically near the axis where it reaches its minimum.

Einstein and Li [E1] developed a theory for a single vortex in a frictionless fluid based on the preservation of moment of momentum as fluid approaches the outlet. This theory leads to infinite velocities at the centre of the vortex.

Wormley [W1] analysed the flow in the vortex chamber by the momentum integral method and showed that the non-dimensional circulation distribution in a short vortex chamber is primarily a function of the geometrical parameter  $BLC^*$  (Modified Boundary Layer Coefficient) for a specified end wall shear law and



velocity profiles. The parameter  $BLC'$  contains the chamber aspect ratio, ratio of outer periphery tangential to radial velocity, Reynolds number and end wall friction coefficient.

Kitsios and Boucher [K2] studied the effect of viscosity in confined vortex flow and reported that, since the effect of viscosity becomes important near the end walls, the decreased tangential velocities in the boundary layers reduce the centrifugal action and the fluid is accelerated inward by the radial pressure gradient. By continuity, this increase in the boundary layer velocity above the core velocity is balanced by a decrease in the core radial velocity itself. Depending on the valve configuration and operating conditions, the radial velocity in a portion of the core may go to zero (giving rise to a 'rotating donut') with all the radial flow occurring in the boundary layers.

Kotas [K3] conducted flow visualization studies and the results demonstrated the three-dimensional nature of the end wall boundary layer flow. Measurement of radial velocities and radial flow balance proved the existence of the reverse radial flow due to flow recirculation between the boundary layer and the main flow. Measurement of the circumferential component of the velocity on the main flow at different radii provided support for a power-law relationship between the velocity and radius.

### 2.3 Non-Dimensional Variables and Characteristic Curves

In evaluating the performance of vortex diodes several non-dimensional variables are considered. Some of the non-dimensional variables are Reynolds number, Euler number, performance ratio and diodicity. Characteristic curves show the relationship between Euler number and Reynolds number over a wide range of diode operation.

The subscript "reverse" in the equations below corresponds to the flow wherein the fluid enters the chamber tangentially and forms a vortex. The subscript "forward" corresponds to the flow wherein it enters axially and leaves the chamber without forming a vortex.

$$\text{Pressure Loss Coefficient (Euler Number)} = \frac{\text{Pressure Drop across Diode}}{0.5 \rho V^2} \quad (2.1)$$

$$\text{Reynolds Number} = \frac{\rho V d}{\mu} \quad (2.2)$$

$$\text{Performance Ratio} = \frac{(\text{Pressure Loss Coefficient})_{\text{reverse}}}{(\text{Pressure Loss Coefficient})_{\text{forward}}} \quad (2.3)$$

(at the same Reynolds Number)

$$\text{Diodicity} = \frac{(\text{Pressure Drop across Diode})_{\text{reverse}}}{(\text{Pressure Drop across Diode})_{\text{forward}}} \quad (2.4)$$

(at the same flow rate)

## CHAPTER III

### EXPERIMENTAL INVESTIGATION

#### 3.1 Introduction

In this chapter a description of the experimental facility and the procedure is presented. The objective of the investigation was to obtain the characteristic curves for flow through vortex diodes in the range  $200 < Re < 3000$ . The pressure drop across the diode was measured using a manometer for different flow rates corresponding to the Reynolds number range under consideration. The flow rates were measured using a set of four rotameters. The Reynolds number was based on the axial pipe diameter as the characteristic length and the average velocity in the axial pipe. The average velocity was calculated by dividing the flow rate by the cross sectional area of the axial pipe. From the flow rate and pressure drop measurements, the non-dimensional pressure loss coefficient (Euler number) corresponding to each Reynolds number considered was calculated. The performance ratio for each Reynolds number was also calculated. The uncertainty associated with each parameter is presented in Appendix A.

Experiments were conducted for both forward (without vortex) and reverse (with vortex) flows for each diode. They were repeated for three geometrically similar diodes. The test fluid was water.

## **3.2 Experimental Equipment**

### **3.2.1 General Test Facility**

This section includes a general description of the closed flow circuit used in the present study. The closed loop design permits the use of a wide variety of fluids, however, for the present investigation, ordinary tap water was used. A schematic diagram of the test facility is presented in Figure 3.1.

Water from a 50 cm x 50 cm x 30 cm reservoir at the floor level was pumped to the upstream constant head tank at a height of about 4 m. The constant head tank is also 50 cm x 50 cm x 30 cm and is fitted with an overflow tube. The tank was supported by a steel frame. Water from the tank passed through a set of rotameters with regulating valves before reaching the test diode. The rotameters were fastened to the steel frame supporting the constant head tank. After passing through the diode the water exited to a collector tank. A thermometer was located in the downstream collector tank. From the collector tank the water drained to the reservoir from which it was pumped back to the constant head tank. The test diode was fastened to a horizontal steel frame which could be adjusted for mounting the different diodes. The pressure drop across the diode was measured with an inclined tube manometer.

A list of equipment used with the least count and range is presented in Appendix B.

### **3.2.2 Rotameters**

Four rotameters were used to measure the range of flow rates corresponding to the Reynolds number range under consideration. The rotameters were connected in series by means of a flexible plastic tubing. The flow rate could be adjusted with ball valves located upstream of the rotameters or the plunger valves downstream. All four rotameters were calibrated individually by measuring the quantity of water collected over a known period of time. The calibration curves obtained by regression analysis of the calibration data are presented in Appendix C. During an experiment the rotameters were flushed of any air bubbles and the readings were recorded after allowing sufficient time for the floats to stabilize.

### **3.2.3 Manometer**

An open tube manometer was used to measure the static pressure upstream and downstream of the diode. Three pressure taps were located on the tangential and axial pipes. The manometer was connected to the pressure taps using flexible plastic tubing. In order to increase the sensitivity, the manometer could be inclined at any required angle to the horizontal. The inclination of the manometer was measured with a digital inclinometer. The entire manometer was mounted on an hydraulic lift mechanism which could be elevated or lowered to accommodate a wide range of pressure measurement.

### **3.2.4 Vortex Diode**

Three vortex diodes, made of Plexiglas, were used for this study. Figure 3.2

shows an isometric view a typical diode. Each vortex diode was constructed from three plates that were fastened together. The central plate contained the vortex chamber and the tangential port (Figure 3.3 and Figure 3.4). The front wall plate contained the axial port. The axial port was attached to the axial pipe and the tangential port to the tangential pipe. The pressure taps were located on the circular pipes upstream and downstream of the diode.

The three diodes were geometrically similar in all the critical dimensions. The dimensions are presented in Table 3.1. The diodes were constructed with an aspect ratio ( $h/D$ ) of 0.4 and radius ratio ( $d/D$ ) of 0.2.

### **3.3 Experimental Procedure**

The lower reservoir was filled with ordinary tap water and the pump was started to transfer the water to the constant head tank. Once the constant tank was full the excess water was returned to the reservoir through the overflow pipe. The manometer was connected to the pressure taps on the diode by means of transparent plastic tubing. The valves on the supply line were opened and the system was flushed to purge air bubbles. Particular care was taken to ensure that there were no bubbles inside the vortex chamber. The valve on the exit side of the diode was then closed, thus forcing the water to flow through the manometer. The tubing from the diode to the manometer as well as the manometer tubes were purged thoroughly of any entrapped air bubbles. The rotameters were calibrated by collecting the discharge over a known period of time and weighing it.

The valves upstream of the diode were adjusted to provide the required flow

rate. Sufficient time was allowed for the flowmeter reading to stabilize. The manometer readings corresponding to the lower menisci were also noted after allowing sufficient time for them to stabilize. The valve downstream of the diode was adjusted, if necessary, in order to vary the level in the manometer. The manometer was inclined at an angle of 5 degrees to the horizontal to increase its sensitivity.

### **3.4 Results and Discussion**

The pressure drops across each of the three diodes are plotted for different flow rates. The pressure drops were plotted for both forward and reverse flows (Figure 3.5 and Figure 3.6). The pressure drop across the smallest diode increased at a higher rate than across the larger diodes.

For the same flow rate, the pressure drop across the diode for reverse flow is greater than that obtained for forward flow. The pressure drop for the reverse flow direction is greater than that for the forward flow direction because of the formation of vortex in the vortex chamber before it exits through the axial port. The pressure drop increases at a greater rate for reverse flow than for forward flow.

From the measurements of flow rates and pressure drops across the diode, the non-dimensional variables Reynolds Number and Euler Number were calculated. The characteristic curves ( $Eu$  vs.  $Re$ ) for all the diodes were drawn on the same graph for comparison. The characteristic curves are shown for both forward and reverse flows in Figures 3.7 and 3.8 respectively.

During forward flow, the fluid enters axially and leaves through the tangential port without forming a vortex. The Euler Number is found to decrease with an increase in Reynolds number (Figure 3.7). This flow is analogous to flow through a pipe with two 90 degree bends.

In the reverse flow direction, the fluid enters the circular chamber through the tangential port and forms a vortex. The Euler number is found to increase with an increase in Reynolds number (Figure 3.8). Flow through the three diodes could not be studied for the entire range of Reynolds Number ( $200 < Re < 3000$ ) because of the limitations in the ranges of pressure and flow rates that could be measured with the equipment used in the experimental study. Empirical relationships between the non-dimensional parameters for the range of Reynolds number considered showed that (Figure 3.9 and Figure 3.10):

For forward flow (no vortex):

$$\ln(Eu) = 24.23 - 8.38 \cdot \ln(Re) \quad (3.1)$$

For reverse flow (with vortex):

$$\ln(Eu) = 3.13 \cdot Re \quad (3.2)$$

When plotted on the same graph, the characteristic curves for the different diodes show no noticeable variation both for the forward and reverse flows. The variation or scatter in the data for the different diodes (Figure 3.7 and Figure 3.8) can be attributed to the uncertainty in the non-dimensional variables due to experimental limitations. Hence it can be concluded that there is no scale effect for the operation of the diodes over the range of Reynolds Number under consideration. The performance ratio shows an increasing trend with increases in



Reynolds Number. Figure 3.11 shows an increasing trend in the performance ratio with increases in Reynolds number. For the Reynolds number range  $200 < Re < 3000$ , the performance ratio is quite poor when compared to values of 40-50 when Reynolds numbers approach magnitudes of  $10^5$ . The performance ratio is found to drop below 1 for Reynolds number less than approx. 400, thus offering higher resistance in the forward flow direction than in the reverse flow direction.

## **CHAPTER IV**

### **NUMERICAL STUDY**

#### **4.1 Introduction**

A computer simulation of a three-dimensional, steady state, incompressible flow through a vortex diode was carried out using the general purpose fluid flow modelling program NISA/3D-FLUID™. A numerical solution to the fluid flow problem was sought because of the lack of any closed form solutions to vortex flow problems. The two most popular numerical schemes available are the finite difference and the finite element schemes.

In the finite difference method the solution domain is divided into a grid of discrete points or nodes and the governing equations for each node are written in finite difference form. The solution is thus obtained by pointwise approximation. This approach has several limitations because it is difficult to apply to systems with irregular geometry, unusual boundary conditions, or nonhomogenous composition. The finite element method provides an alternative that is better suited for such systems. In contrast to finite difference techniques, the finite element method divides the solution domain into simply shaped regions or elements. An approximate solution for the partial differential equation is developed for each of these elements. The total solution is then generated by linking together or assembling the individual solutions taking care to ensure continuity at the inter-element boundaries. Thus the solution is obtained in a piecewise fashion. The use of elements, rather than a rectangular grid, provides a much better approximation for irregularly shaped systems. Further, values of the dependent variable can be

generated continuously across the entire solution domain rather than at isolated points [C1].

#### 4.2 NISA/3D-FLUID™

NISA/3D-FLUID™ is a general purpose, interactive, fluid flow modelling program. It can be used for solving both boundary and initial value problems. The equations of motion governing fluid flow with heat transfer are given by the Continuity equation

$$\frac{\partial \rho}{\partial t} + \frac{\partial}{\partial x_k} (\rho u_k) = 0 \quad (4.1)$$

Momentum equation

$$\rho \left[ \frac{\partial u_i}{\partial t} + u_k \frac{\partial u_i}{\partial x_k} \right] = -\frac{\partial p}{\partial x_i} + \frac{\partial}{\partial x_i} \left( \lambda \frac{\partial u_k}{\partial x_k} \right) + \frac{\partial}{\partial x_j} \left[ \mu \left( \frac{\partial u_i}{\partial x_j} + \frac{\partial u_j}{\partial x_i} \right) \right] + \rho f_i \quad (4.2)$$

Energy equation

$$\rho C_v \left[ \frac{\partial T}{\partial t} + u_k \frac{\partial T}{\partial x_k} \right] = -p \frac{\partial u_k}{\partial x_k} + \frac{\partial}{\partial x_j} \left( K \frac{\partial T}{\partial x_j} \right) + \Phi + \rho q_s \quad (4.3)$$

It uses the finite element technique for solving the equations which govern fluid flow with heat transfer. The technique involves subdivision of the solution domain into many smaller regions of convenient shapes, such as triangles, quadrangles and hexahedrons and uses an approximation method to quantify the behaviour of

each element. Suitable local co-ordinate systems are specified for each element, and the governing differential equations are replaced by an approximation using values of the dependent variables at the nodes. Using the Galerkin weighted residual method, the governing differential equations are transformed into finite element equations governing each isolated element. These local equations are collected together to form a global system of algebraic equations including a proper accounting of boundary conditions. The nodal values of the dependent variables are determined from the solution of this matrix equation. The Gauss-elimination method is used for solving the matrix equation. Figure 4.1 shows the flow chart for NISA fluid flow analysis.

The NISA/3D FLUID™ program consists of three modules: Preprocessing, Analysis and Postprocessing modules. In the preprocessing module the finite elements are generated for the required geometry. The boundary conditions and properties of the fluid are also specified in this section. In the analysis module the finite element equations are solved and the nodal values of the dependent variables are obtained. In the postprocessing module a graphical representation of the results is obtained. The values of the dependent variables at the individual nodes at the inlet and outlet sections can also be obtained in this module.

### **4.3 Finite Element Modelling**

The numerical simulation of asymmetric flow through the vortex diode was carried out in the following phases:

#### **4.3.1 Discretization**

In this phase, using the preprocessing module, the three-dimensional geometry of the smallest diode was modelled with the same dimensions as that of the test diode. Due to difficulties encountered in specifying the boundary conditions, the diode was modelled in two parts. The first part, which consists of the vortex chamber, the axial port and the rectangular tangential port is shown in Figure 4.2. The second part consisting of the transition from circular pipe to rectangular tangential port is shown in Figure 4.3. To prevent a discontinuity in the calculated values in the model, care was taken to ensure that the nodes at boundaries of different geometric shapes matched with each other. The geometry was divided into 1628 elements with 1898 nodes. The 8-noded hexahedral brick element shown in Figure 4.4 was selected from the NISA/3D-FLUID™ element library. The element description is given in Table 4.1.

#### **4.3.2 Boundary Conditions**

A Dirichlet type of boundary condition was applied at the boundary nodes by specifying the values of the three components of velocity. The walls of the diode were specified by giving a value of zero to all three components of velocities. For the inlet nodes the average velocity at the inlet pipe, corresponding to the Reynolds number of the flow under consideration was calculated and specified. All

other components were set to zero.

### 4.3.3 Finite Element Equations

NISA/3D-FLUID™ uses the continuity, Navier-Stokes and energy equations for solving incompressible flow problems. The governing differential equations for incompressible laminar flow can be written as

$$\frac{\partial u_k}{\partial x_k} = 0 \quad (4.4)$$

$$\rho \left( \frac{\partial u_i}{\partial t} + u_k \frac{\partial u_i}{\partial x_k} \right) = -\frac{\partial p}{\partial x_i} + \frac{\partial}{\partial x_j} \left[ \mu \left( \frac{\partial u_i}{\partial x_j} + \frac{\partial u_j}{\partial x_i} \right) \right] + \rho f_i \quad (4.5)$$

$$\rho C_v \left( \frac{\partial T}{\partial t} + u_k \frac{\partial T}{\partial x_k} \right) = \frac{\partial}{\partial x_j} \left( k \frac{\partial T}{\partial x_j} \right) + \phi + \rho q_s \quad (4.6)$$

$$\phi = \mu \left( \frac{\partial u_i}{\partial x_j} + \frac{\partial u_j}{\partial x_i} \right) \frac{\partial u_j}{\partial x_i} \quad (4.7)$$

The objective of the finite element method is to approximate the differential

equations by a system of algebraic equations. Within each element, the dependent variables, velocity, pressure and temperature, are approximated in terms of simple polynomial shape functions. The coefficients of these polynomials are obtained from the values of the dependent variable at the nodes. Mathematically, the velocity, pressure and temperature in an element can be written as

$$u_i(x,t) = \psi u_i(t) \quad (4.8)$$

$$p(x,t) = \varphi p(t) \quad (4.9)$$

$$T(x,t) = \theta T(t) \quad (4.10)$$

where the unknowns  $u_i, p$  and  $T$  are column vectors at nodal points and  $\psi, \varphi$  and  $\theta$  are column vectors of the shape functions. Substituting these relationships into the governing equations yields a set of equations of the form

$$f(\psi, \varphi, \theta, u_i, p, T) = R \quad (4.11)$$

where  $R$  is the residual resulting from the use of approximations.

In order to obtain an optimal solution, which seeks to reduce the error (residual  $R$ ) to zero, the Galerkin form of weighted residuals is used. This is done by achieving orthogonality between the residual  $R$  and the weighting function  $w$  of the element. This condition requires that is expressed as

$$\int_{\Omega_e} (L \cdot w) d\Omega = \int_{\Omega_e} (R \cdot w) d\Omega = 0 \quad (4.12)$$

where  $w$  is the weighting function and  $\Omega_e$  is the element domain.

The outcome of this method is analogous to curve fitting. Instead of fitting functions to data, however, it specifies in an optimal fashion, the relationship

between the coefficients of the polynomial shape function which satisfy the underlying partial differential equation in an optimal fashion.

The resulting element equations consist of a set of algebraic equations that can be expressed in the form

$$[m] \{\dot{u}\} + [k] \{u\} = \{s\} \quad (4.13)$$

where  $[m]$  is the mass matrix,  $[k]$  is the non-linear stiffness matrix of the fluid,  $\{u\}$  is the nodal velocity,  $\{s\}$  is the source vector, and  $\{\dot{u}\}$  is the derivative of  $u$  with respect to time.

#### 4.3.4 Assembly and Solution

After the individual element equations were derived, they were linked together to characterize the behavior of the entire system. The assembly process was governed by the concept of continuity. After final assembly, the entire system can be expressed in the form

$$[M] \{\dot{U}\} + [K] \{U\} = \{S\} \quad (4.14)$$

where  $[M]$  and  $[K]$  are the assembled mass and stiffness matrices respectively.  $\{\dot{U}\}$ ,  $\{U\}$  and  $\{S\}$  are the column vectors obtained after assembly of vectors  $\{\dot{u}\}$ ,  $\{u\}$  and  $\{s\}$  from individual elements. A solution to the above equation was obtained by the Gauss-elimination method of decomposition.



#### **4.3.5 Postprocessing**

In this phase, a graphical representation of the results was obtained. The nodal values of the pressures at the inlet and outlet pipe walls were obtained and the pressure drops calculated.

#### **4.4 Results**

Numerical results were obtained for different Reynolds numbers varying from 200 to 3000 for flows with vortex (tangential entry) and without vortex (axial entry) for Diode 1. The program was run on a Sun SPARCstation2™ with 32MB memory and speed of 27 Mips. The total pressure drop across the diode, corresponding to the pressure drop measured experimentally, was obtained by adding the pressure drops across the two parts modelled separately. The average pressures at the inlet and at the outlet were obtained by taking the average of four pressure readings at four different wall nodes. When the model was analyzed with 3495 nodes instead of 1898 nodes, a difference of 2% in the pressure was observed at  $Re = 1000$ . The pressure drop obtained was non-dimensionalized to give the Euler number by using the velocity at the axial port as the reference velocity. The characteristic curve was obtained by plotting the resulting Euler number against the corresponding Reynolds number.

Figure 4.5 and Figure 4.6 show comparisons of the pressure drops obtained numerically and experimentally for the forward and reverse flow respectively for

Diode 1. There is a fairly good agreement between the experimental data and the numerical results for both forward and reverse flows. The non-dimensionalized parameters were compared by plotting the characteristic curves for both experimental and numerical values for the forward and reverse flow cases respectively in Figure 4.7 and Figure 4.8. At lower Reynolds numbers ( $Re < 1000$ ) the variation between the two curves is greater than at higher Reynolds numbers. This difference can be attributed to the greater uncertainty in the experimental values at lower Reynolds numbers.

The performance ratio of diode 1 was calculated for the range of Reynolds numbers considered and plotted against Reynolds numbers as shown in Figure 4.9. The figure shows that performance ratio increases with increasing Reynolds number.

#### 4.5 Discussion

The three-dimensional asymmetric finite element modelling and analysis of the vortex diode for Reynolds numbers in the range  $200 < Re < 3000$  yielded good agreement with the experimental results. The numerical analysis by the finite element method presents an excellent alternative to the simplified analytical models obtained by assuming inviscid flow. Different shapes of the vortex diode can be analyzed, e.g., with nozzles or diffusers at the inlet and outlet, with vortex chamber of different aspect ratios ( $h/D$ ) and radius ratios ( $d/D$ ) and their effects on performance can be evaluated. This study can be used for developing an optimum design procedure. The effects of fluids with different properties (such as non-Newtonian fluids) can also be studied without extensive experimentation.

## CHAPTER V

### SUMMARY OF CONCLUSIONS AND RECOMMENDATIONS

#### 5.1 Conclusions

The conclusions from the present study can be summarised as follows:

- 1) There is no noticeable scale effect over the range of Reynolds number considered, i.e., the size of the diode does not influence the performance the diode provided that geometric similarity is preserved.
- 2) The non-dimensional variables, Euler number and Reynolds number are found to be sufficient to describe the flow characteristics.
- 3) From the experimental study empirical relationships were obtained between the non-dimensional variables (Eu and Re) for the range of Reynolds number considered.
- 4) For flows at low Reynolds Number the performance ratio of the vortex diode is quite low thus limiting its application.
- 5) The results obtained by numerical modelling shows good agreement with the experimental results. Thus numerical models could be used for studying the characteristics of vortex diodes with different structural and flow conditions.
- 6) Below  $Re \approx 400$ , the performance drops below 1, i.e., the diode offers higher resistance in the forward flow than in the reverse flow direction.

## **5.2 Recommendations**

Some recommendations for future studies are as follows:

- 1) The experimental study should be conducted with more accurate pressure measuring and flow rate measuring devices to reduce the uncertainty.
- 2) Confined vortex flow patterns inside the vortex chamber should be studied by flow visualization techniques.
- 3) The performance of the vortex diode should be studied with alternate or modified designs which might offer a higher performance ratio at low Reynolds number.
- 4) Studies should be conducted on the operation of vortex diodes with non-Newtonian fluids.

## REFERENCES

- B1 BAKER, P. J., 1967, "A comparison of Fluid Diodes", *Proceedings of the 2<sup>nd</sup> Cranfield Fluidics Conference*, Cambridge. U.K. pp 63-72
- B2 BROMACH, H., and NEUMAYER, H., 1977, "Development of a Very Large Radial Vortex Valve", *Fluidics Quarterly*, Vol. 9, No. 2, pp 59-75
- C1 CHAPRA, N., and STEVEN, C., 1988, *Numerical Methods for Engineers*, McGraw Hill, New York
- E1 EINSTIEN, K., and LI, M., 1951, "Steady Vortex Flow in a Real Fluid", *Proceedings of the Heat Transfer and Fluid Mechanics Institute*, Stanford, CA, pp. 33-43
- E2 ETHERINGTON, C., 1984, "Power Fluidics Technology and its Application in the Nuclear Industry", *Nuclear Energy*, Vol. 23, No. 4, pp 227-235
- F1 FINEBLUM, S. S., 1974, "Vortex Diodes", *Fluidics State-of-the-art Symposium*, Harry Diamond Labs., Washington, D.C., Vol. 1, pp 45-80
- G1 GEORGE, P. J., WARD, J. R., and MITCHELL, F. M., 1975, "Vortex Diode Characteristics at High Pressure Ratios", *Proceeding of the Conference Organised by Institute of Measurement and Control*, London, Paper No.9
- H1 HOLMAN, J. P., *Experimental Methods for Engineers*, 1984, 4<sup>th</sup> Edition, McGraw Hill, New York
- J1 JACOBS, B. E. A., and BAKER, P. J., 1972, "The Steady-state and Transient Performance of Some Large-Scale Vortex Diodes", *Proceedings of 5<sup>th</sup> Cranfield Fluidics Conference*, Uppsala, Sweden, Paper E2

- K1 KIRSHNER, J. M., 1975, "Design Theory of Fluidic Components", Academic Press, New York
- K2 KITSIOS, E. E. and BOUCHER, R. F., 1985, "The Dynamics of Vortex Amplifiers", *Journal of Dynamic Systems, Measurement and Control*, Vol. 107, pp. 176-181
- K3 KOTAS, T. J., 1975, "Turbulent Boundary Layer Flow on the End Wall of a Cylindrical Vortex Chamber, *Journal of Heat Transfer and Fluid Flow*, Vol. 5, No. 2, pp. 77-87
- M1 McMUIGAN, J. A. K., and BOUCHER, R. F., 1973, "A Fluidic Rectifier for Pumping", *Proceedings of the Symposium on Power Fluidics for Process Control*, pp. 97-104
- N1 NISA/3D-FLUID™, User's Manual, 1990, Engineering Mechanics Research Corporation, Troy, Michigan
- P1 PRIESTMAN, G. H., and TIPPETTS, J. R., 1984, "*Development and Potential of Power Fluidics for Process Flow Control*", Vol. 6, No. 2, pp. 68-80
- R1 REYDON, R. F. and GAUVIN, W. H., 1981, "Theoretical and Experimental Studies of Confined Vortex Flow", *The Canadian Journal of Chemical Engineering*, Vol. 59, pp. 14-23
- S1 SIDHU, B. S., SYRED, N. and STYLES, A. C., 1980, "Flow and General Characteristics of High Performance Diodes", ASME Winter Annual Meeting, *Vortex Flows*, pp. 113-122

- T1 TIPPETTS, J. R., PRIESTMAN, G. H. and THOMPSON D., 1981,  
"Development in Power Fluidics for Application in Nuclear Plant", *Journal of Dynamic Systems, Measurement and Control*, Vol. 103, pp. 342-351
- V1 VATISTAS, G. H., LIN, S. and KWOK, C. K., 1986, "Theoretical and Experimental Studies on Vortex Chamber Flows", *AIAA Journal*, Vol. 24, No. 4, pp. 635-642
- W1 WORMLEY D. N., 1969, "An Analytical Model for the Incompressible Flow in Short Vortex Chambers", *Journal of Basic Engineering*, 68-WA/FE-17, pp. 264-276
- W2 WORMLEY D. N., 1976, "A Review of Vortex Diode and Triode Static and Dynamic Design Characteristics", *Fluidics Quarterly*, Vol. 8, No. 1, pp. 85-112



## FIGURES

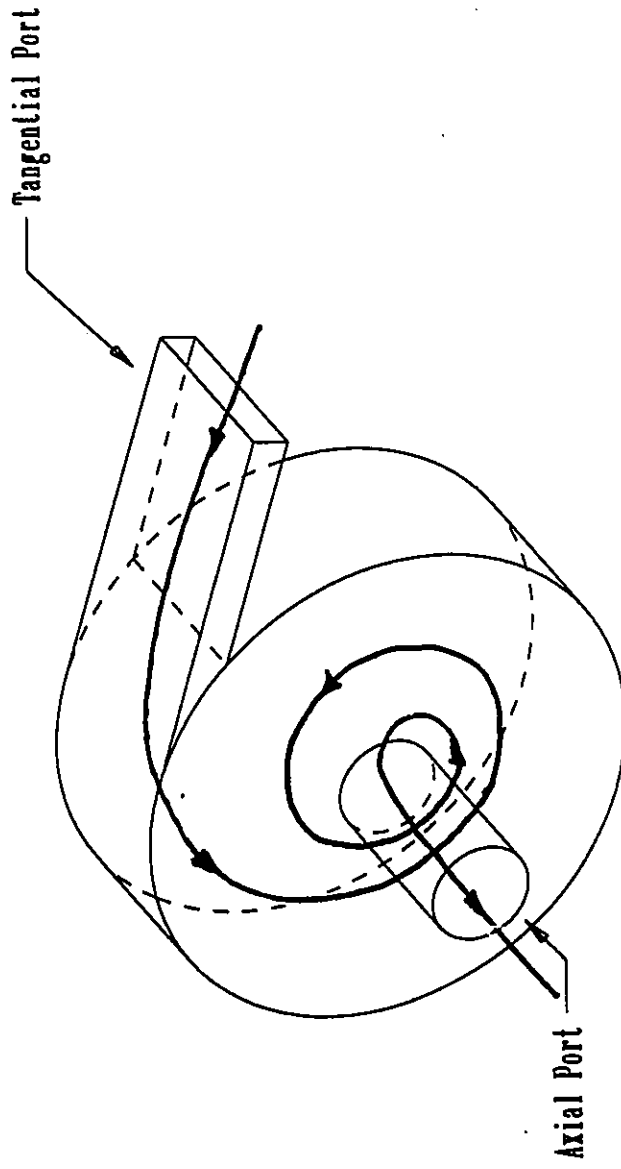


**Figure 1.1 Reverse Flow**

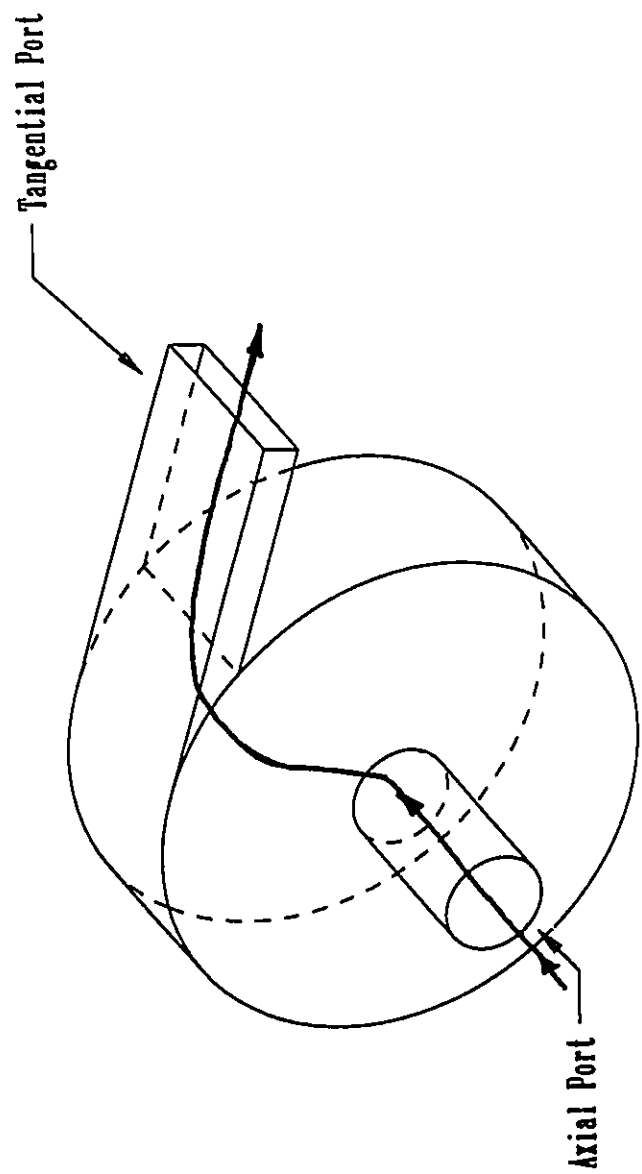
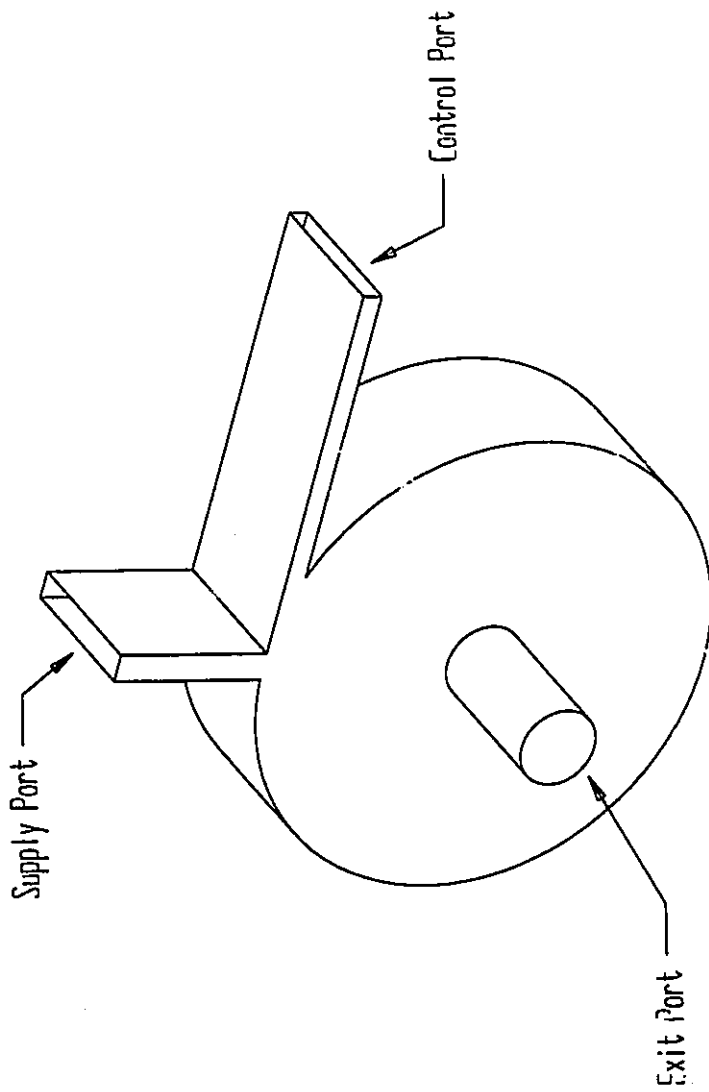
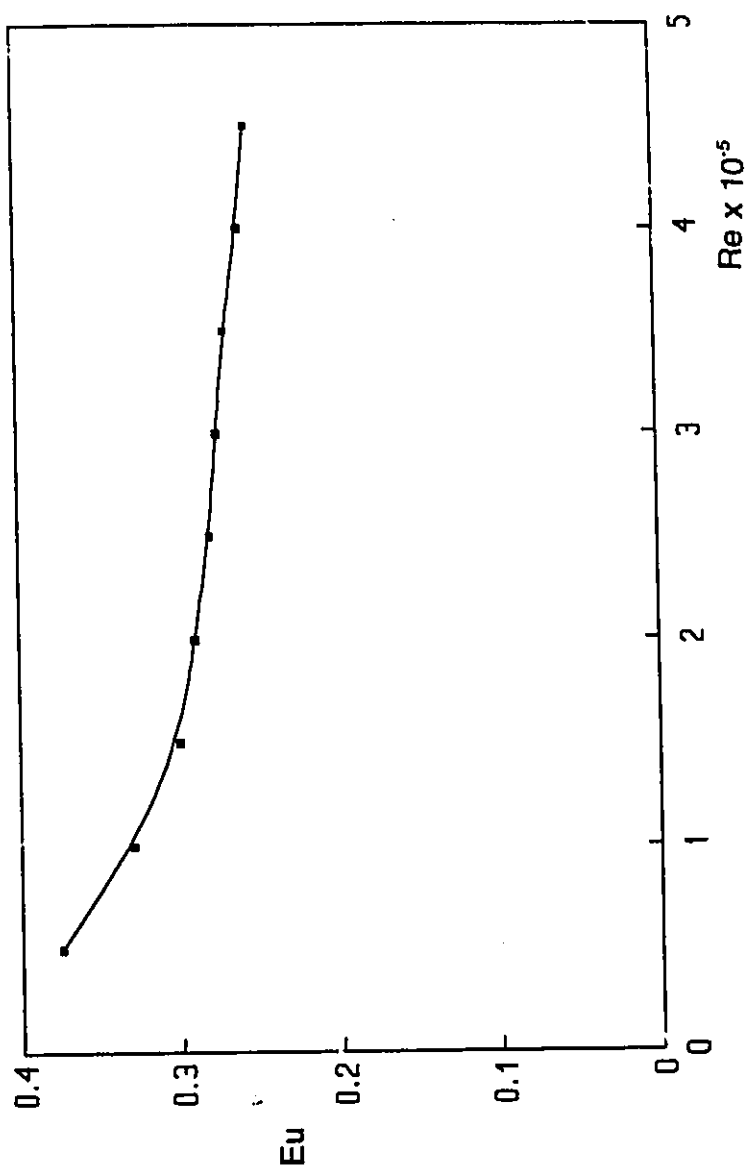


Figure 1.2 Forward Flow



**Figure 2.1** Vortex Amplifier



**Figure 2.2** Characteristic Curve (Zobel Diode) Forward Flow [P1]

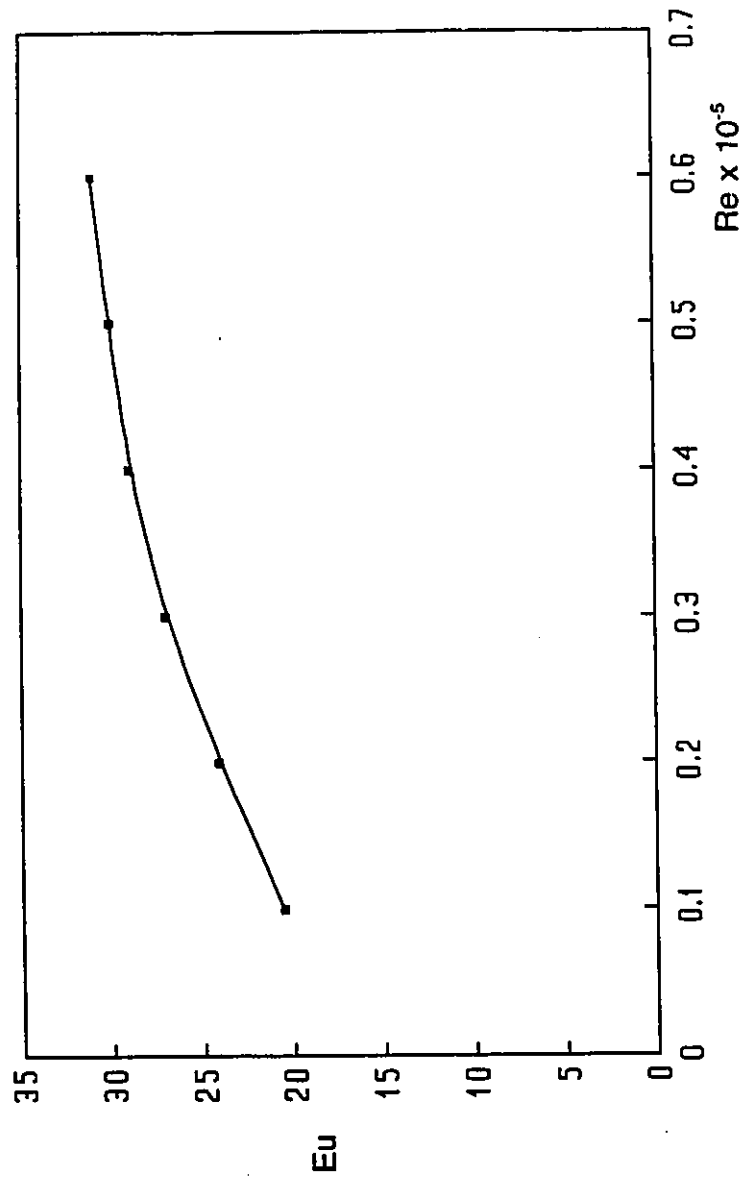


**Figure 2.3** Characteristic Curve (Zobel Diode) Reverse Flow [P1]

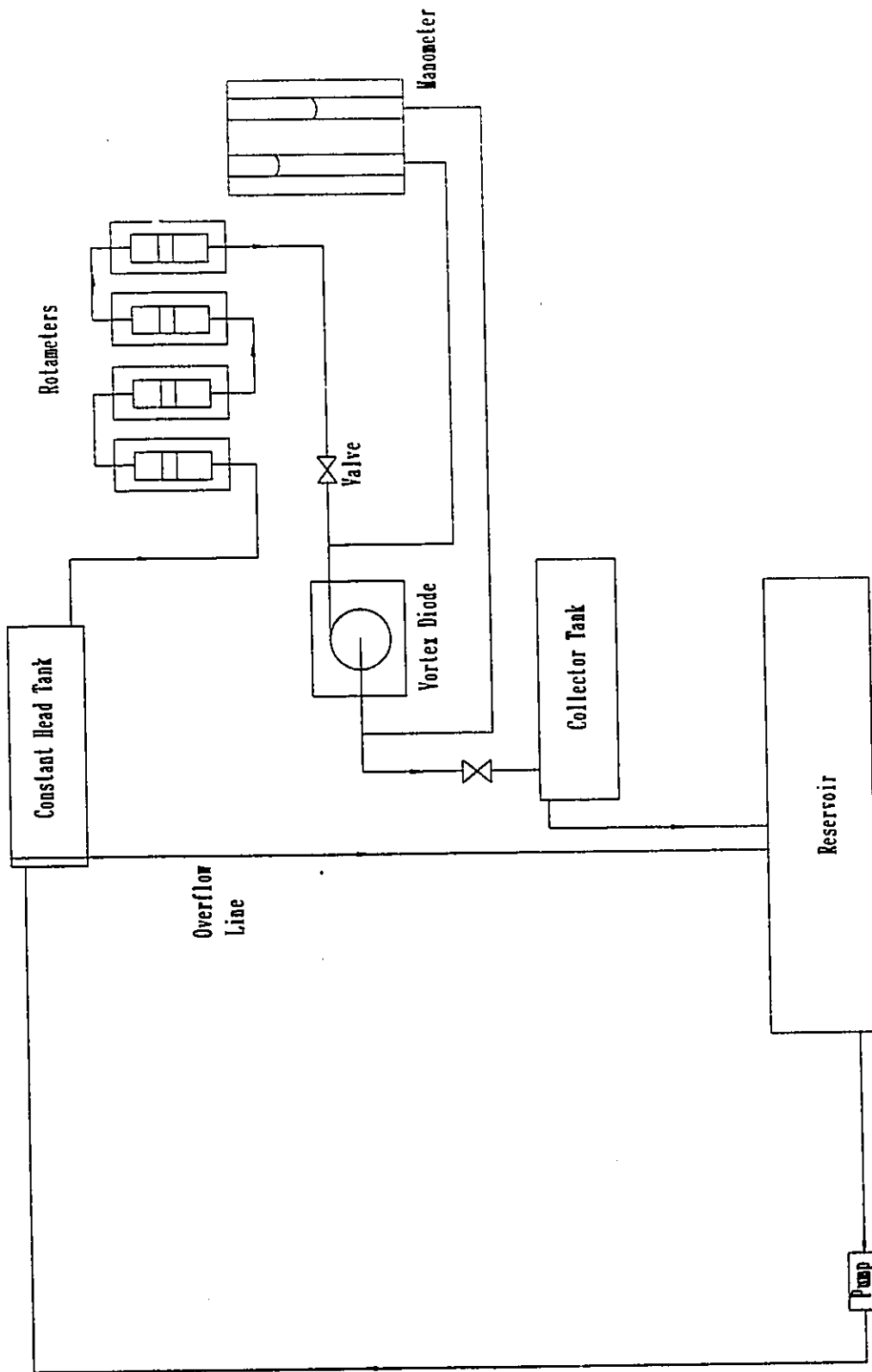


Figure 3.1 Schematic Diagram of Test Facility

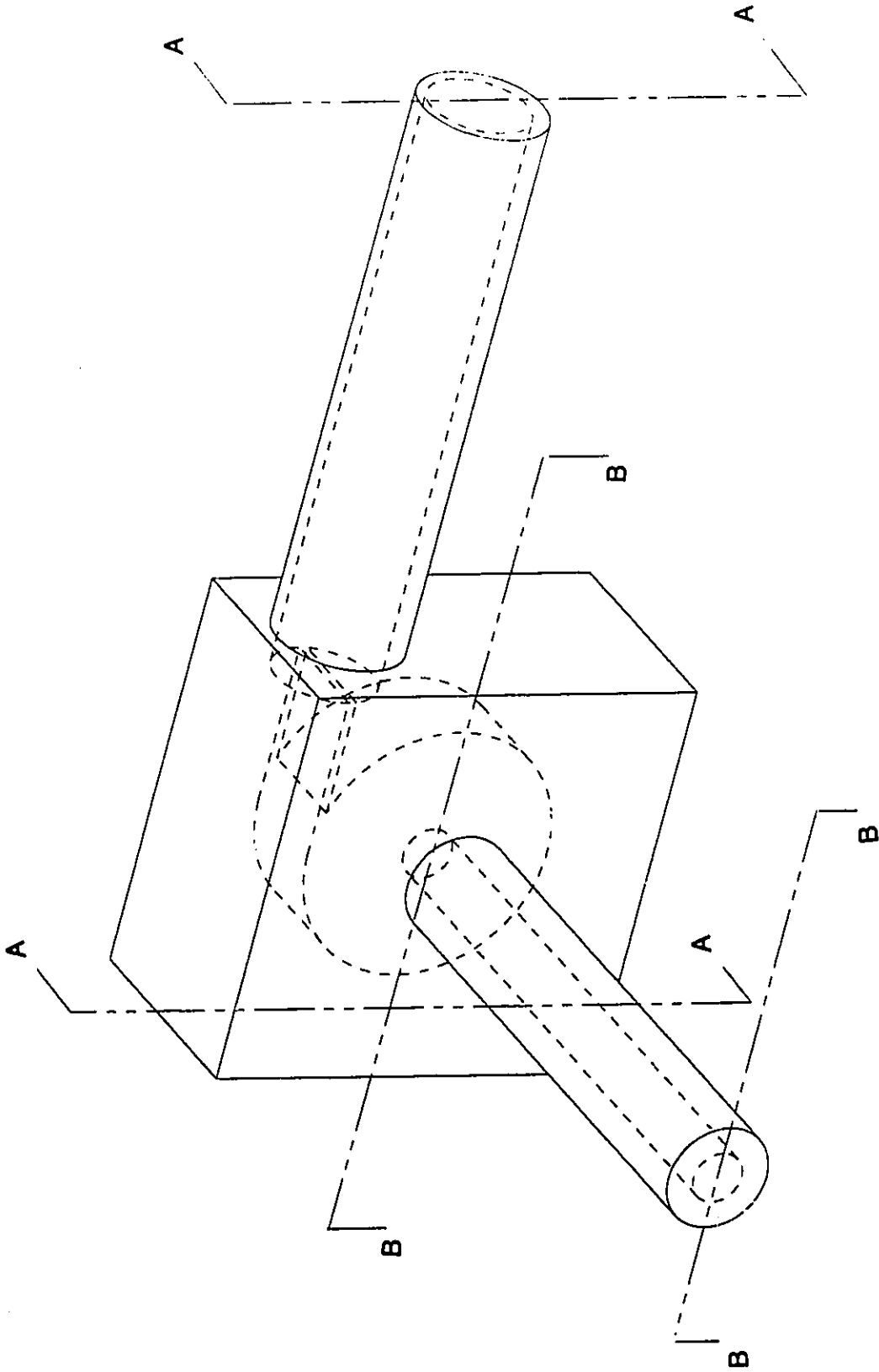


Figure 3.2 Isometric View of Test Diode



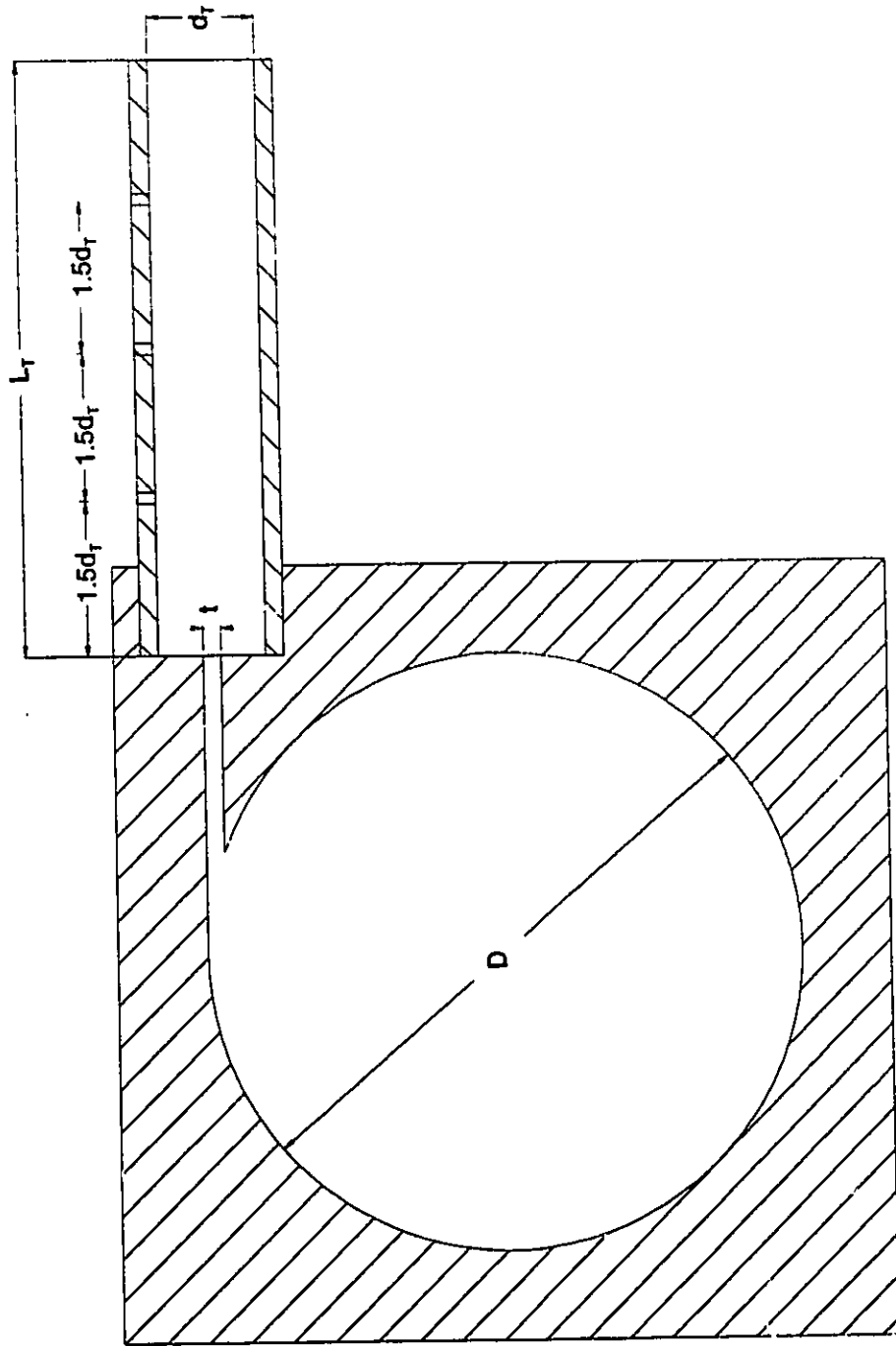


Figure 3.3 Section A - A

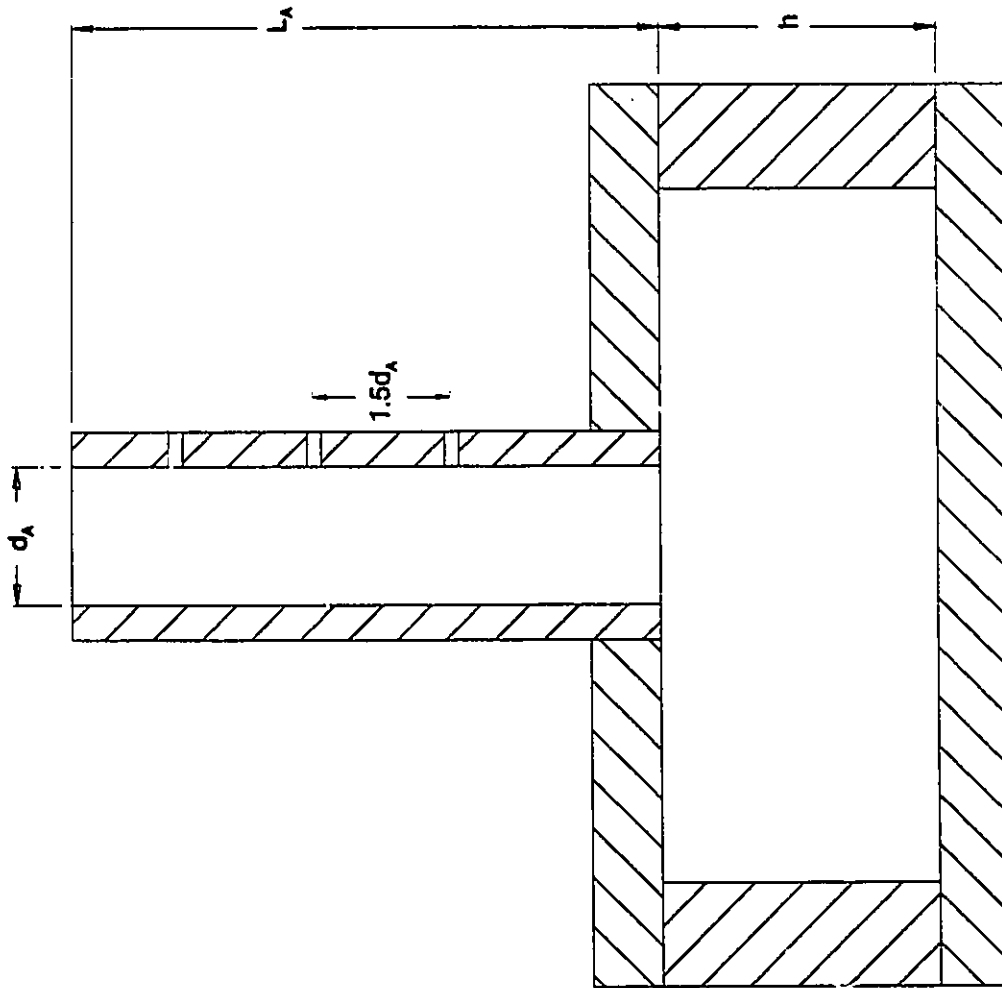


Figure 3.4 Section B - B

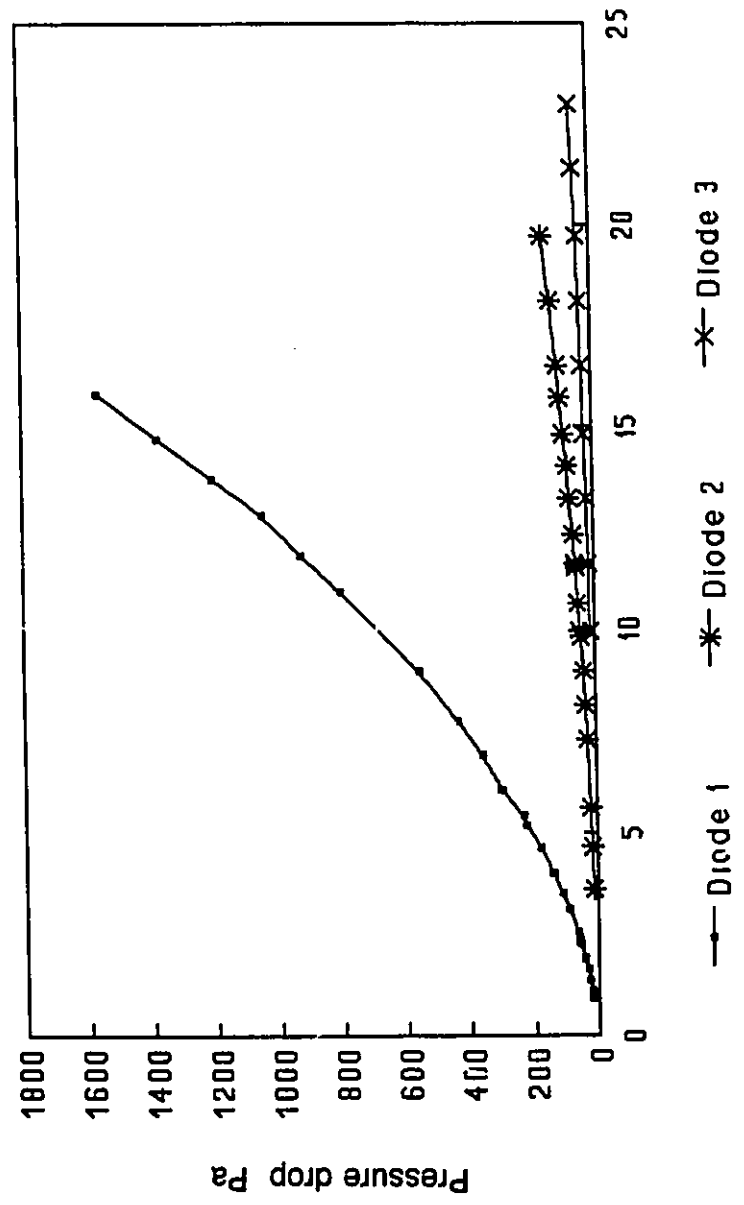


Figure 3.5 Pressure Drop Vs. Flow Rate (Forward Flow)

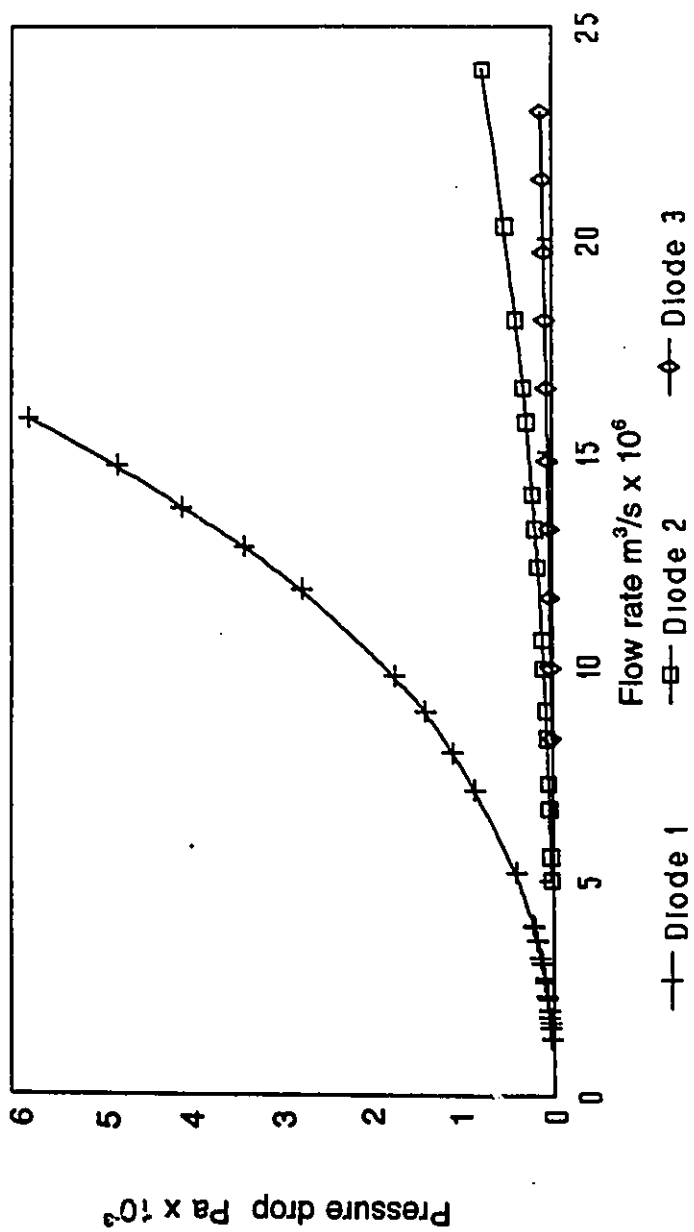


Figure 3.6 Pressure Drop Vs. Flow Rate (Reverse Flow)

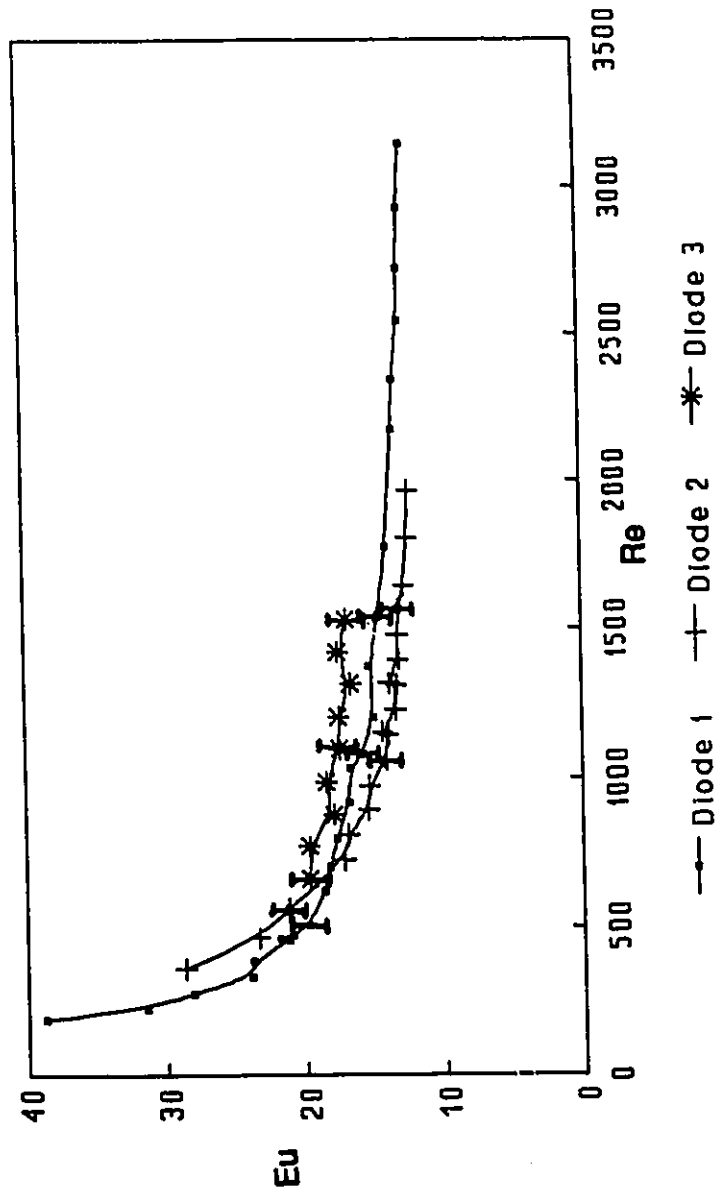


Figure 3.7 Characteristic Curve (Forward Flow)

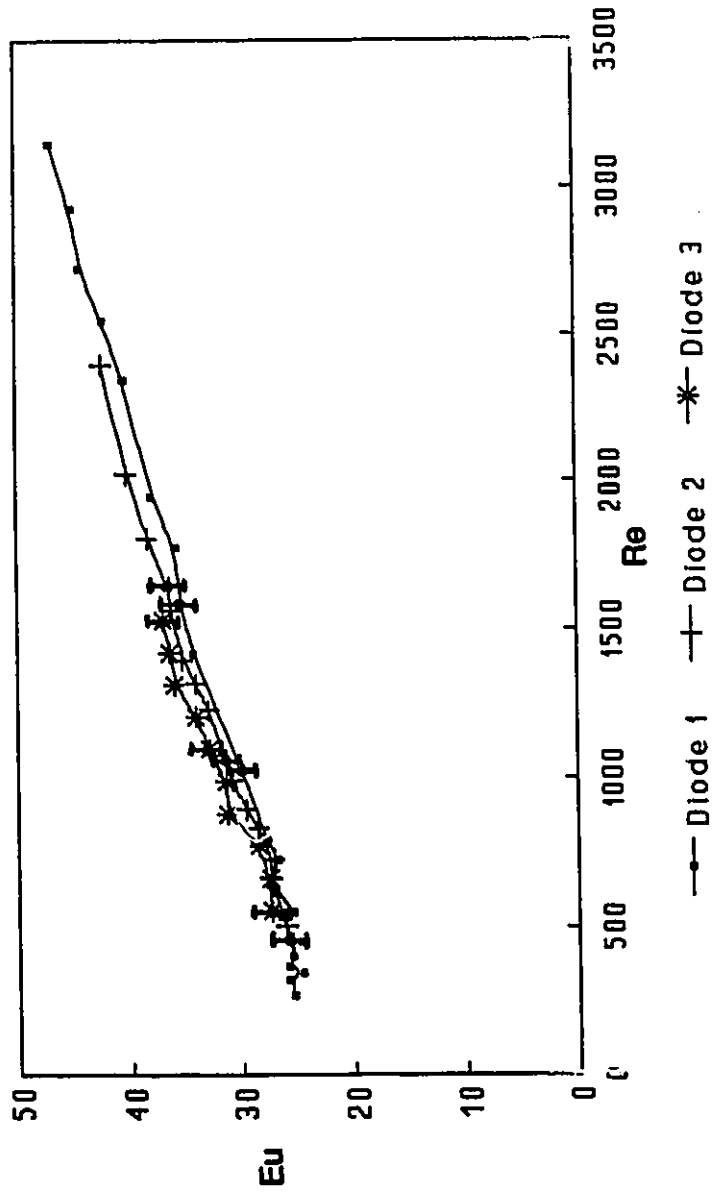


Figure 3.8 Characteristic Curve (Reverse Flow)

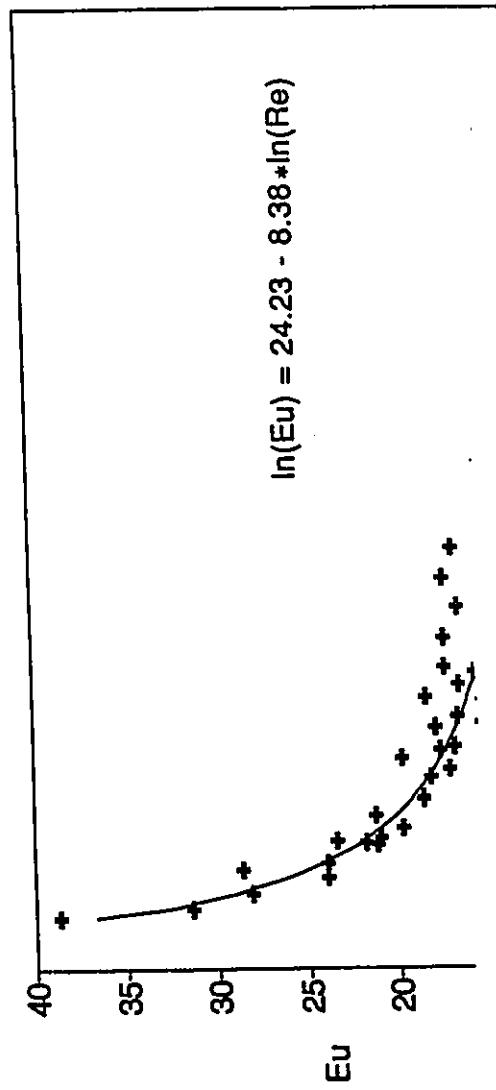


Figure 3.9 Best-fit Curve (Forward Flow)

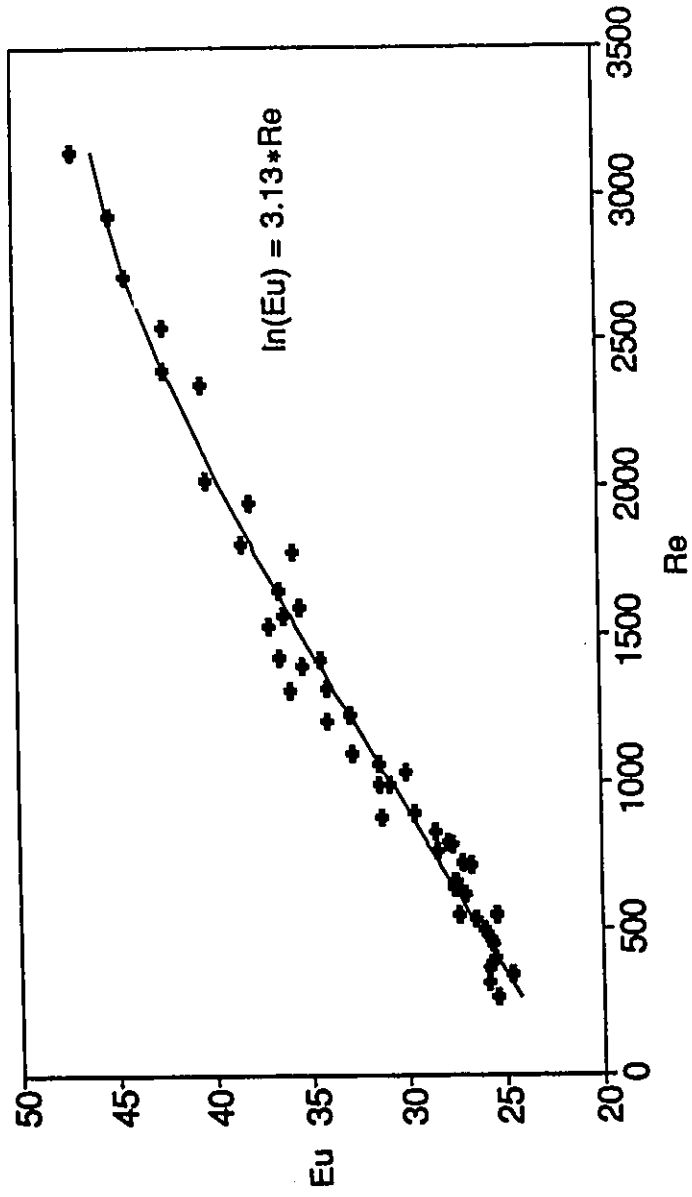


Figure 3.10 Best-fit Curve (Reverse Flow)



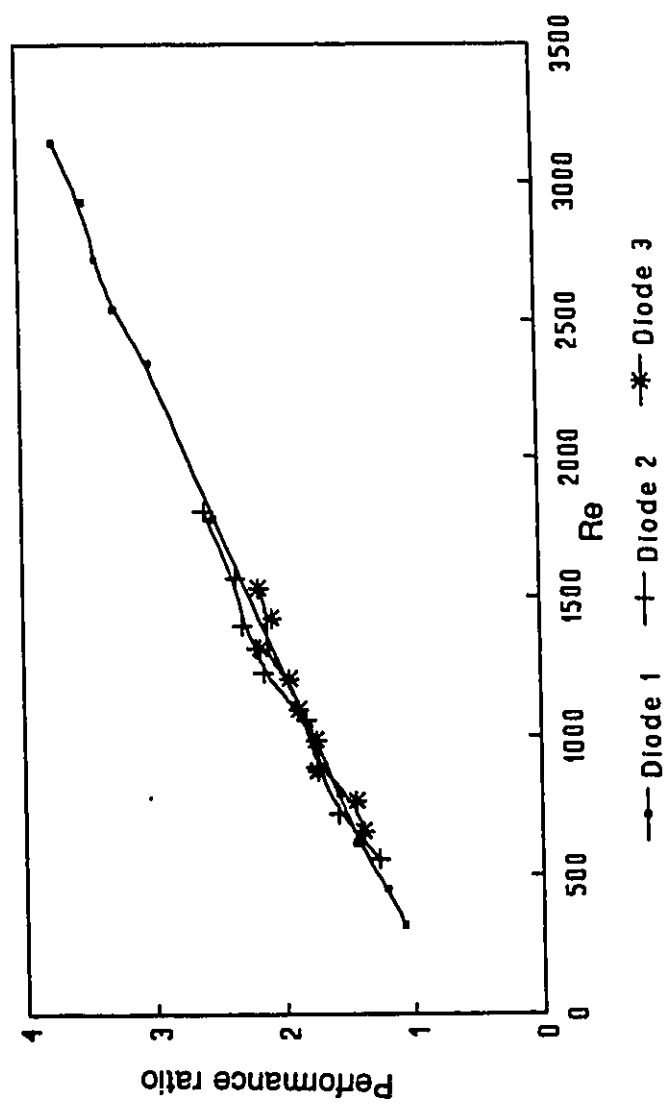
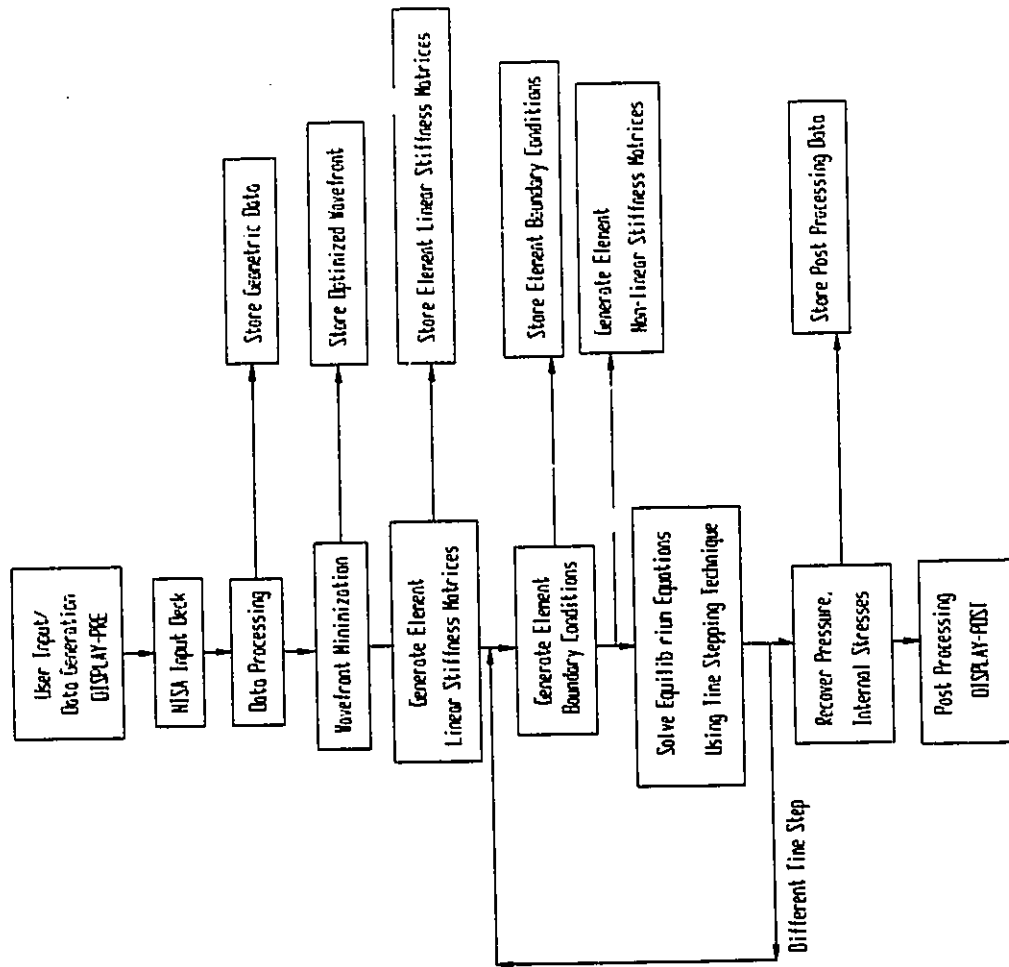
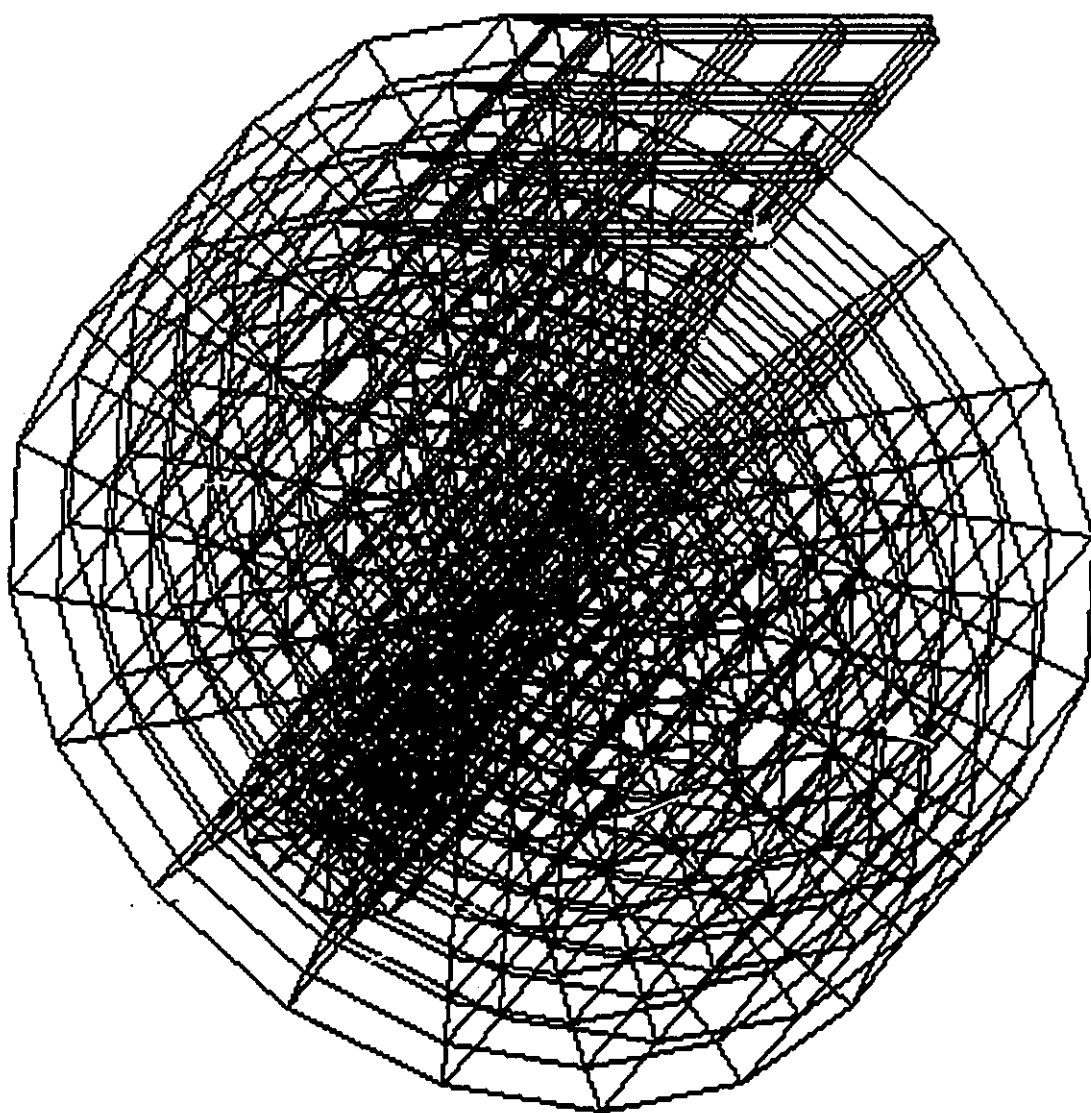


Figure 3.11 Performance Ratio Vs. Reynolds Number



**Figure 4.1** NISA Fluid Flow Analysis Flow Chart [N1]



**Figure 4.2** Finite Element Discretization of Vortex Chamber

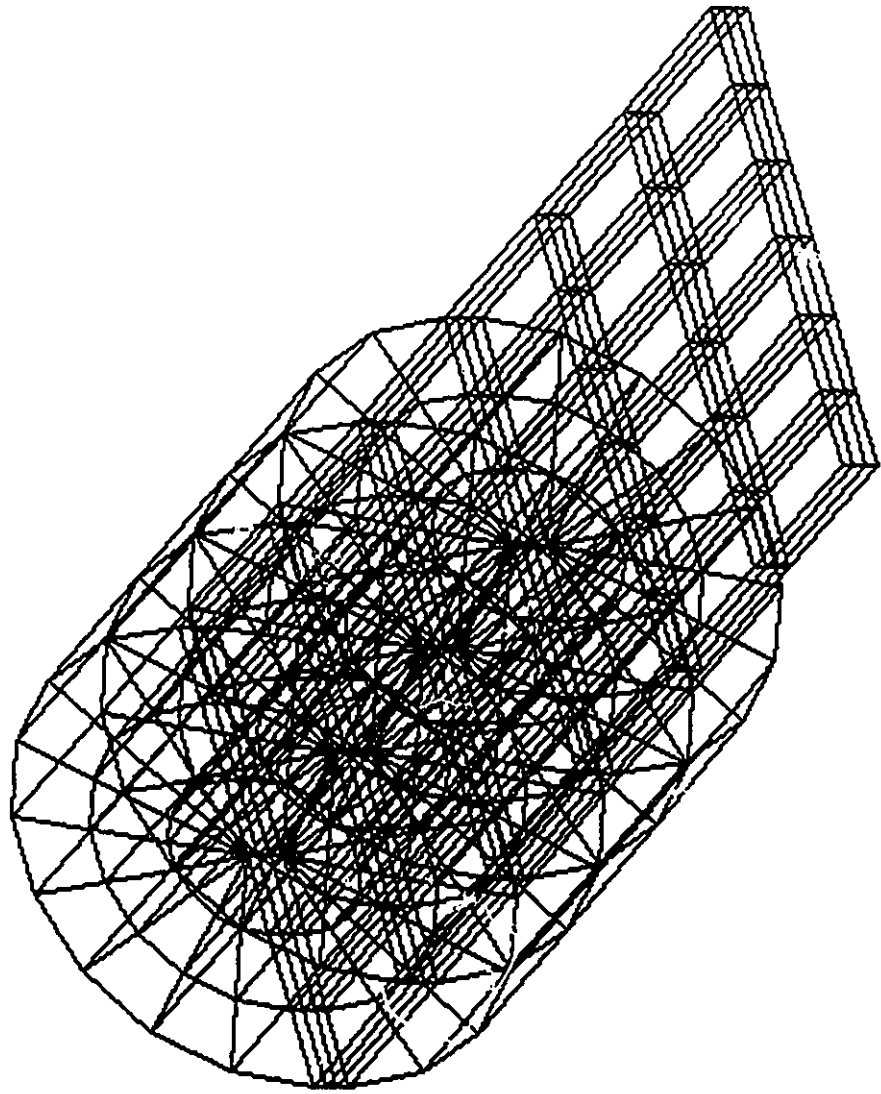
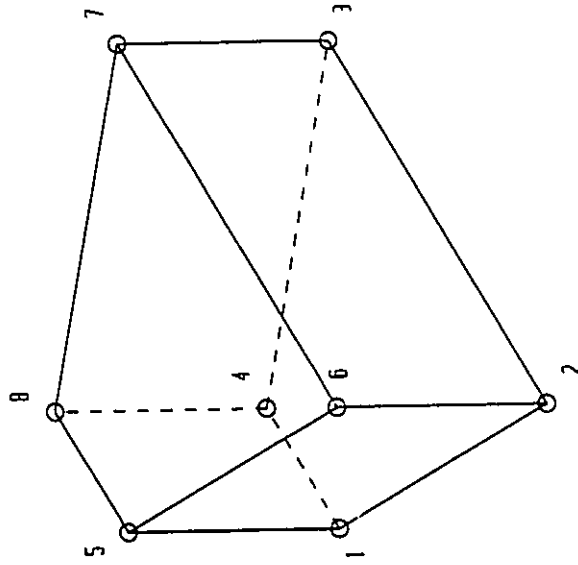


Figure 4.3 Finite Element Discretization of Tangential Inlet



**Figure 4.4** 8-Noded Hexahedral Element

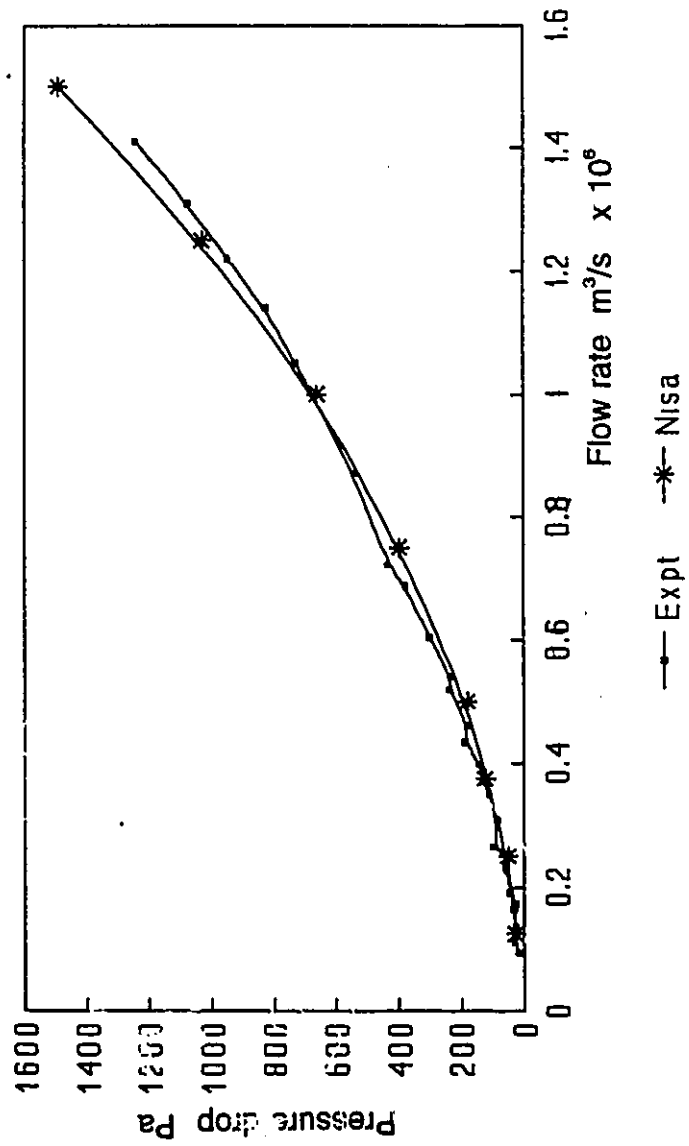


Figure 4.5 Comparison of Numerical Solution (Diode 1) Forward Flow

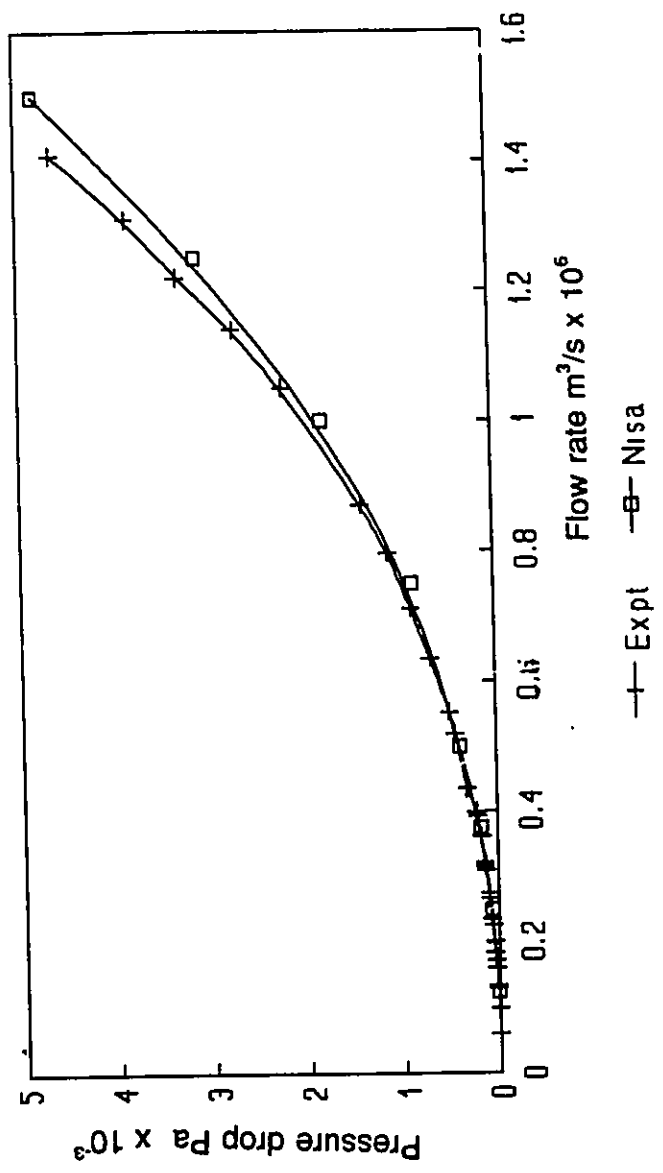


Figure 4.6 Comparison of Numerical Solution (Diode 1) Reverse Flow

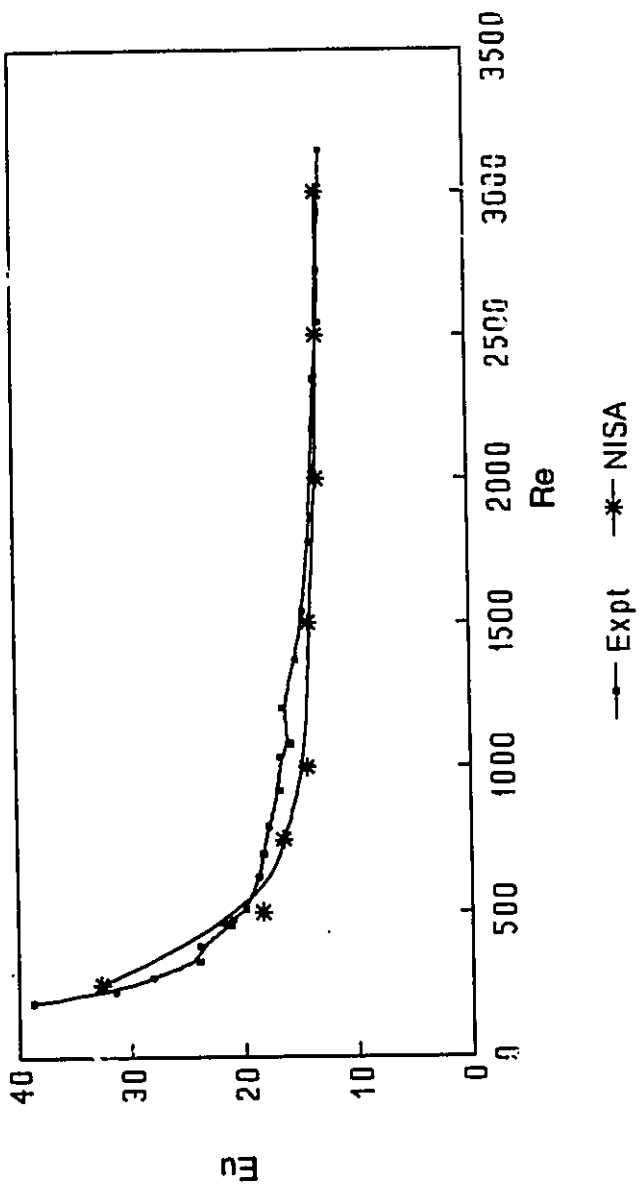


Figure 4.7 Characteristic Curve (Diode 1) Forward Flow



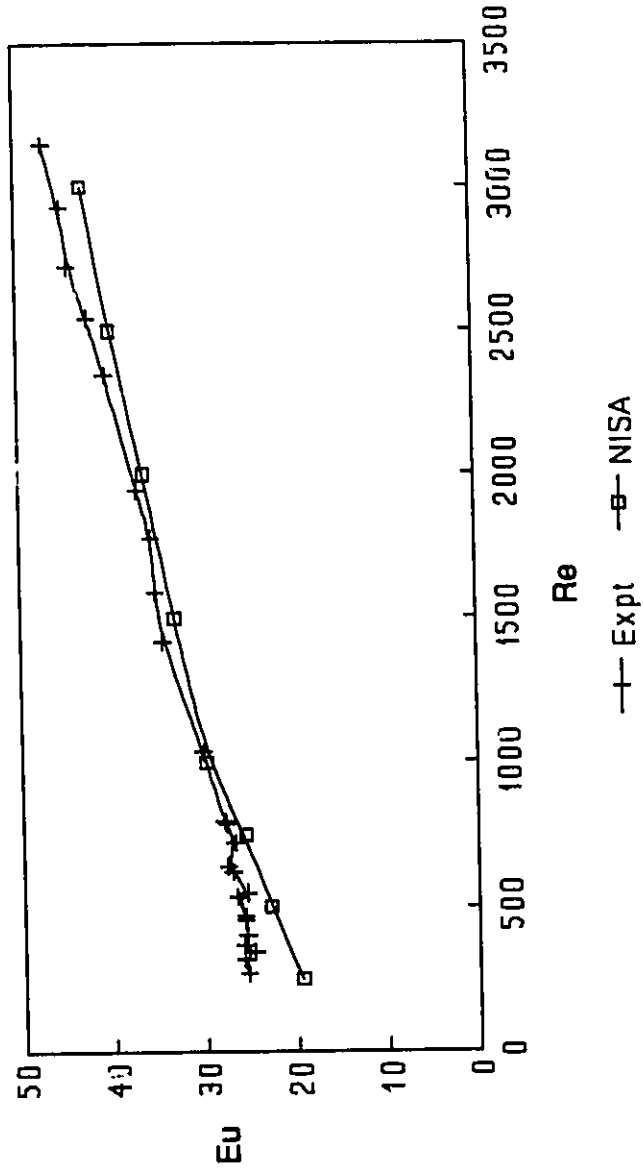


Figure 4.8 Characteristic Curve (Diode 1) Reverse Flow

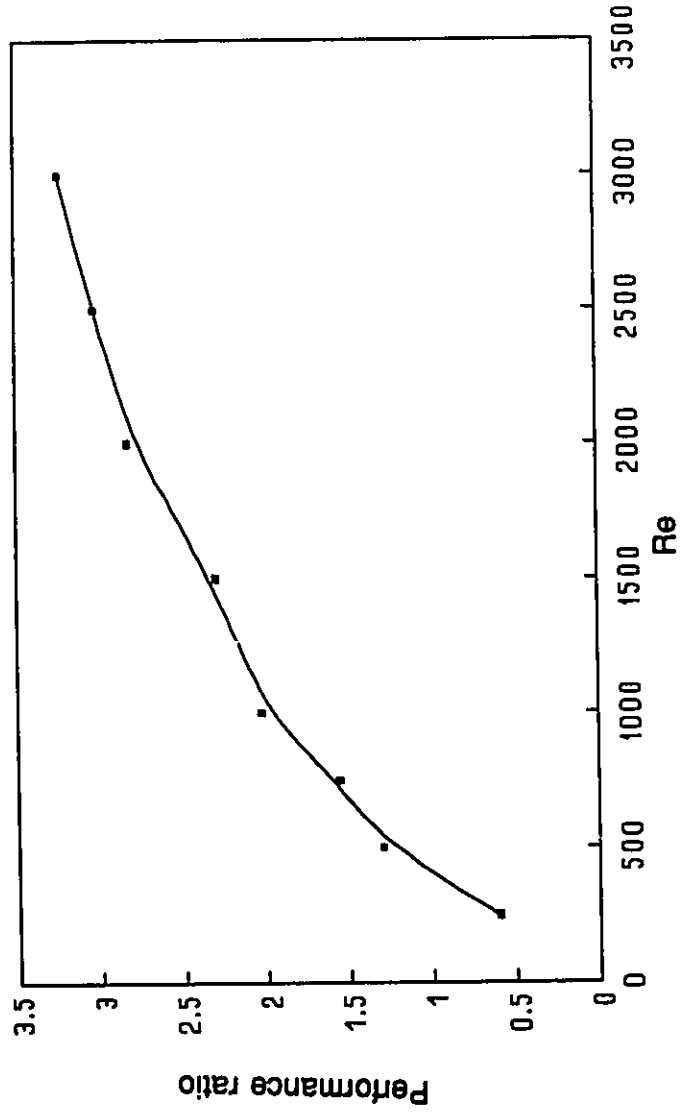


Figure 4.9 Performance ratio Vs. Re No.

## **TABLES**

Diode No.	$h$ ( $10^{-3}\text{m}$ )	$D$ ( $10^{-3}\text{m}$ )	$d_A$ ( $10^{-3}\text{m}$ )	$d_T$ ( $10^{-3}\text{m}$ )	$L_A$ ( $10^{-3}\text{m}$ )	$L_T$ ( $10^{-3}\text{m}$ )	$t$ ( $10^{-3}\text{m}$ )
Diode 1	12.7	31.75	6.35	12.7	90	120	1
Diode 2	25.4	63.50	12.70	25.4	180	240	2
Diode 3	38.1	95.25	19.05	38.1	270	360	3

**Table 3.1** Dimensions of Test Diodes

Element type	3 Dimensional element
Analysis type	Fluid
Degrees of freedom	3 per node: $u, v, w$
Shape	Hexahedron (Brick)
Number of nodes	8
Material properties	Density, viscosity, conductivity and temperature
Nodal Boundary Conditions	Velocity components $u, v, w$ at the node

**Table 4.1** Element Description

**APPENDIX A**  
**UNCERTAINTY ANALYSIS**

## UNCERTAINTY ANALYSIS

The procedure developed by Kline and McClintock [H1] was used for the uncertainty analysis. The uncertainties in the variables were assumed to have the same odds. The uncertainties in the primary experimental measurements were estimated to be one half of the smallest division unless otherwise specified by the manufacturer. The uncertainty is denoted by 'W' and subscripted with the quantity being considered.

The uncertainty in the dependent variable R is expressed as:

$$W_R = \left[ \left( \frac{\partial R}{\partial x_1} \cdot W_1 \right)^2 + \left( \frac{\partial R}{\partial x_2} \cdot W_2 \right)^2 + \dots + \left( \frac{\partial R}{\partial x_n} \cdot W_n \right)^2 \right]^{1/2} \quad (\text{A.1})$$

where  $R = R(x_1, x_2, \dots, x_n)$  and  $W_1, W_2, \dots, W_n$  are the uncertainties in the measurement of  $x_1, x_2, \dots, x_n$  respectively.

The relative uncertainty in R is obtained by rearranging the above equation and to the form:

$$\frac{W_R}{R} = \left[ \left( \frac{\partial R}{\partial x_1} \cdot \frac{W_1}{R} \right)^2 + \left( \frac{\partial R}{\partial x_2} \cdot \frac{W_2}{R} \right)^2 + \dots + \left( \frac{\partial R}{\partial x_n} \cdot \frac{W_n}{R} \right)^2 \right]^{1/2} \quad (\text{A.2})$$

In this section the uncertainty analysis in the quantities V,  $\Delta p$ ,  $\Delta p_r$ , Re,  $Eu$ ,  $Eu_r$  and Performance Ratio for Diode 1 at a Reynolds number of 500 is considered.

**Axial Velocity V:**

$$V = \frac{4Q}{\pi d^2} \quad (\text{A.3})$$

where  $d = (6.35 \pm 0.05) \times 10^{-5} \text{ m}$

$Q = (2.506 \pm 0.0925) \times 10^{-6} \text{ m}^3/\text{s}$

$$W_V = \left[ \left( \frac{\partial V}{\partial Q} \cdot W_Q \right)^2 + \left( \frac{\partial V}{\partial d} \cdot W_d \right)^2 \right]^{1/2} \quad (\text{A.4})$$

The relative uncertainty is given by:

$$\frac{W_V}{V} = \left[ \left( \frac{W_Q}{Q} \right)^2 + 4 \left( \frac{W_d}{d} \right)^2 \right]^{1/2} \quad (\text{A.5})$$

which gives  $V = (0.07913 \pm 0.0032) \text{ m/s}$  ( $\pm 4.1\%$ )

**Head drop across diode (Forward flow)  $h_t$**

$$h_t = h_i - h_o \quad (\text{A.6})$$

where  $h_i = (0.342 \pm 0.001) \text{ m}$

$h_o = (0.268 \pm 0.001) \text{ m}$

$$W_{h_t} = \left[ \left( \frac{\partial h_t}{\partial h_i} \cdot W_{h_i} \right)^2 + \left( \frac{\partial h_t}{\partial h_o} \cdot W_{h_o} \right)^2 \right]^{1/2} \quad (\text{A.7})$$



The relative uncertainty is given by:

$$\frac{W_{h_f}}{h_f} = \left[ \left( \frac{W_{h_1}}{h_f} \right)^2 + \left( \frac{W_{h_0}}{h_f} \right)^2 \right]^{1/2} \quad (\text{A.8})$$

which gives  $h_f = 0.074 \pm 0.0014 \text{ m}$  ( $\pm 1.9\%$ )

**Pressure drop across diode (Forward flow)  $\Delta p_f$**

$$\Delta p_f = \rho g h_f \sin \theta \quad (\text{A.9})$$

where  $\theta = 5 \pm 0.1$  degrees

$$h_f = 0.074 \pm 0.0014 \text{ m}$$

$$\rho = 998 \pm 0.119 \text{ kg/m}^3$$

$$W_{\Delta p_f} = \left[ \left( \frac{\partial \Delta p_f}{\partial \rho} \cdot W_\rho \right)^2 + \left( \frac{\partial \Delta p_f}{\partial h_f} \cdot W_{h_f} \right)^2 + \left( \frac{\partial \Delta p_f}{\partial \theta} \cdot W_\theta \right)^2 \right]^{1/2} \quad (\text{A.10})$$

The relative uncertainty is given by:

$$\frac{W_{\Delta p_f}}{\Delta p_f} = \left[ \left( \frac{W_\rho}{\rho} \right)^2 + \left( \frac{W_{h_f}}{h_f} \right)^2 + \left( \frac{W_\theta}{\theta} \right)^2 \right]^{1/2} \quad (\text{A.11})$$

which gives  $\Delta p_f = 62.72 \pm 1.73 \text{ Pa}$  ( $\pm 2.7\%$ )

**Head drop across diode (Reverse flow)  $h_r$**

$$h_r = h_i - h_o \quad (\text{A.12})$$

where  $h_i = (0.199 \pm 0.001) \text{ m}$

$h_o = (0.103 \pm 0.001) \text{ m}$

$$W_{h_r} = \left[ \left( \frac{\partial h_r}{\partial h_i} \cdot W_{h_i} \right)^2 + \left( \frac{\partial h_r}{\partial h_o} \cdot W_{h_o} \right)^2 \right]^{1/2} \quad (\text{A.13})$$

The relative uncertainty is given by:

$$\frac{W_{h_r}}{h_r} = \left[ \left( \frac{W_{h_i}}{h_i} \right)^2 + \left( \frac{W_{h_o}}{h_o} \right)^2 \right]^{1/2} \quad (\text{A.14})$$

which gives  $h_r = 0.096 \pm 0.0014 \text{ m}$  ( $\pm 1.47\%$ )

**Pressure drop across diode (Reverse flow)  $\Delta p_r$**

$$\Delta p_r = \rho g h_r \sin \theta \quad (\text{A.15})$$

where  $\theta = 5 \pm 0.1 \text{ degrees}$

$h_r = 0.096 \pm 0.0014 \text{ m}$

$\rho = 998 \pm 0.119 \text{ kg/m}^3$

$$W_{\Delta p_r} = \left[ \left( \frac{\partial \Delta p_r}{\partial \rho} \cdot W_\rho \right)^2 + \left( \frac{\partial \Delta p_r}{\partial h_r} \cdot W_{h_r} \right)^2 + \left( \frac{\partial \Delta p_r}{\partial \theta} \cdot W_\theta \right)^2 \right]^{1/2} \quad (\text{A.16})$$

The relative uncertainty is given by:

$$\frac{W_{\Delta p_r}}{\Delta p_r} = \left[ \left( \frac{W_\rho}{\rho} \right)^2 + \left( \frac{W_{h_r}}{h_r} \right)^2 + \left( \frac{W_\theta}{\theta} \right)^2 \right]^{1/2} \quad (\text{A.17})$$

which gives  $\Delta p_r = 81.97 \pm 2.03 \text{ Pa}$  ( $\pm 2.48\%$ )

### Reynolds Number Re

$$Re = \frac{\rho V d}{\mu} \quad (\text{A.18})$$

where  $\rho = 998 \pm 0.119 \text{ kg/m}^3$

$V = (0.07913 \pm 0.0032) \text{ m/s}$

$d = (6.35 \pm 0.05) \times 10^{-3} \text{ m}$

$\mu = (1.003 \pm 0.0103) \times 10^{-3} \text{ Pa sec}$

$$W_{Re} = \left[ \left( \frac{\partial Re}{\partial \rho} \cdot W_\rho \right)^2 + \left( \frac{\partial Re}{\partial V} \cdot W_V \right)^2 + \left( \frac{\partial Re}{\partial d} \cdot W_d \right)^2 + \left( \frac{\partial Re}{\partial \mu} \cdot W_\mu \right)^2 \right]^{1/2} \quad (\text{A.19})$$

The relative uncertainty is given by:

$$\frac{W_{Re}}{Re} = \left[ \left( \frac{W_p}{\rho} \right)^2 + \left( \frac{W_v}{V} \right)^2 + \left( \frac{W_d}{d} \right)^2 + \left( \frac{W_\mu}{\mu} \right)^2 \right]^{1/2} \quad (\text{A.20})$$

which gives  $Re = 500 \pm 19.5$  ( $\pm 4.2\%$ )

**Pressure Loss Coefficient or Euler Number (Forward flow)  $Eu_f$**

$$Eu_f = \frac{\Delta p_f}{0.5 \rho V^2} \quad (\text{A.21})$$

where  $\Delta p_f = 62.72 \pm 1.73$  Pa

$$\rho = 998 \pm 0.119 \text{ kg/m}^3$$

$$V = (0.07913 \pm 0.0032) \text{ m/s}$$

$$W_{Eu_f} = \left[ \left( \frac{\partial Eu_f}{\partial \Delta p_f} \cdot W_{\Delta p_f} \right)^2 + \left( \frac{\partial Eu_f}{\partial \rho} \cdot W_\rho \right)^2 + \left( \frac{\partial Eu_f}{\partial V} \cdot W_V \right)^2 \right]^{1/2} \quad (\text{A.22})$$

The relative uncertainty is given by:

$$\frac{W_{Eu_f}}{Eu_f} = \left[ \left( \frac{W_{\Delta p_f}}{\Delta p_f} \right)^2 + \left( \frac{W_\rho}{\rho} \right)^2 + 4 \left( \frac{W_V}{V} \right)^2 \right]^{1/2} \quad (\text{A.23})$$

which gives  $Eu_f = 20.09 \pm 1.73$  ( $\pm 8.63\%$ )

Pressure Loss Coefficient or Euler Number (Reverse flow)  $Eu_r$ ,

$$Eu_r = \frac{\Delta p_r}{0.5 \rho V^2} \quad (\text{A.24})$$

where  $\Delta p_r = 81.97 \pm 2.03$  Pa

$$\rho = 998 \pm 0.119 \text{ kg/m}^3$$

$$V = (0.07913 \pm 0.0032) \text{ m/s}$$

$$W_{Eu_r} = \left[ \left( \frac{\partial Eu_r}{\partial \Delta p_r} \cdot W_{\Delta p_r} \right)^2 + \left( \frac{\partial Eu_r}{\partial \rho} \cdot W_{\rho} \right)^2 + \left( \frac{\partial Eu_r}{\partial V} \cdot W_V \right)^2 \right]^{1/2} \quad (\text{A.25})$$

The relative uncertainty is given by:

$$\frac{W_{Eu_r}}{Eu_r} = \left[ \left( \frac{W_{\Delta p_r}}{\Delta p_r} \right)^2 + \left( \frac{W_{\rho}}{\rho} \right)^2 + 4 \left( \frac{W_V}{V} \right)^2 \right]^{1/2} \quad (\text{A.26})$$

which gives  $Eu_r = 26.07 \pm 2.23$  ( $\pm 8.56\%$ )

**Performance Ratio P.R.**

$$P.R. = \frac{Eu_r}{Eu_f} \quad (\text{A.27})$$

where  $Eu_f = 20.09 \pm 1.73$

$$Eu_r = 26.07 \pm 2.23$$

$$W_{P.R.} = \left[ \left( \frac{\partial F.R.}{\partial EU_f} \cdot W_{EU_f} \right)^2 + \left( \frac{\partial P.R.}{\partial EU_r} \cdot W_{EU_r} \right)^2 \right]^{1/2} \quad (A.28)$$

The relative uncertainty is given by:

$$\frac{W_{P.R.}}{P.R.} = \left[ \left( \frac{W_{EU_f}}{EU_f} \right)^2 + \left( \frac{W_{EU_r}}{EU_r} \right)^2 \right]^{1/2} \quad (A.29)$$

which gives      Performance Ratio P.R. = 1.29 ± 0.156    (±12.15%)

**APPENDIX B**  
**EQUIPMENT TABLE**

01227

EQUIPMENT TABLE

DESCRIPTION	MAKE	LEAST COUNT	RANGE
Weighing Machine	Computer Electronic	0.0001 kg	0 - 2 kg.
Manometer	T.E.M.	2 cm	0 - 60 cm.
Rotameter 1	Rota Oeflingen	$0.15 \times 10^{-6}$ $m^3/s$	0 - $3 \times 10^{-6}$ $m^3/s$
Rotameter 2	Rota Oeflingen	$0.18 \times 10^{-6}$ $m^3/s$	0 - $4.5 \times 10^{-6}$ $m^3/s$
Rotameter 3	Gilmont	$0.4 \times 10^{-6}$ $m^3/s$	0 - $16 \times 10^{-6}$ $m^3/s$
Rotameter 4	Gilmont	$0.8 \times 10^{-6}$ $m^3/s$	0 - $25 \times 10^{-6}$ $m^3/s$
Stopwatch	Cole-Parmer	0.01 sec.	0 - 100 min.
Thermometer	Fisher	1°C	-20°C - 50°C
Inclinometer	Sperry	0.1°	0 - 360°



**APPENDIX C**  
**ROTAMETER CALIBRATION**

## ROTAMETER CALIBRATION

The four rotameters used in the experimental investigation were calibrated using water at 21°C.

The equations of best-fit curves obtained by regression analysis for the calibration data of the rotameters are given below:

### Rotameter 1

$$\text{Flow rate (m}^3/\text{s)} = 1.549 \times 10^{-7} * \text{Reading} - 2.834 \times 10^{-7}$$

### Rotameter 2

$$\text{Flow rate (m}^3/\text{s)} = 2.2906 \times 10^{-7} * \text{Reading} - 3.866 \times 10^{-7}$$

### Rotameter 3

$$\text{Flow rate (m}^3/\text{s)} = 1.6857 \times 10^{-5} * \text{Reading} + 5.09 \times 10^{-7}$$

### Rotameter 4

$$\text{Flow rate (m}^3/\text{s)} = 1.6356 \times 10^{-5} * \text{Reading} + 1.754 \times 10^{-6}$$

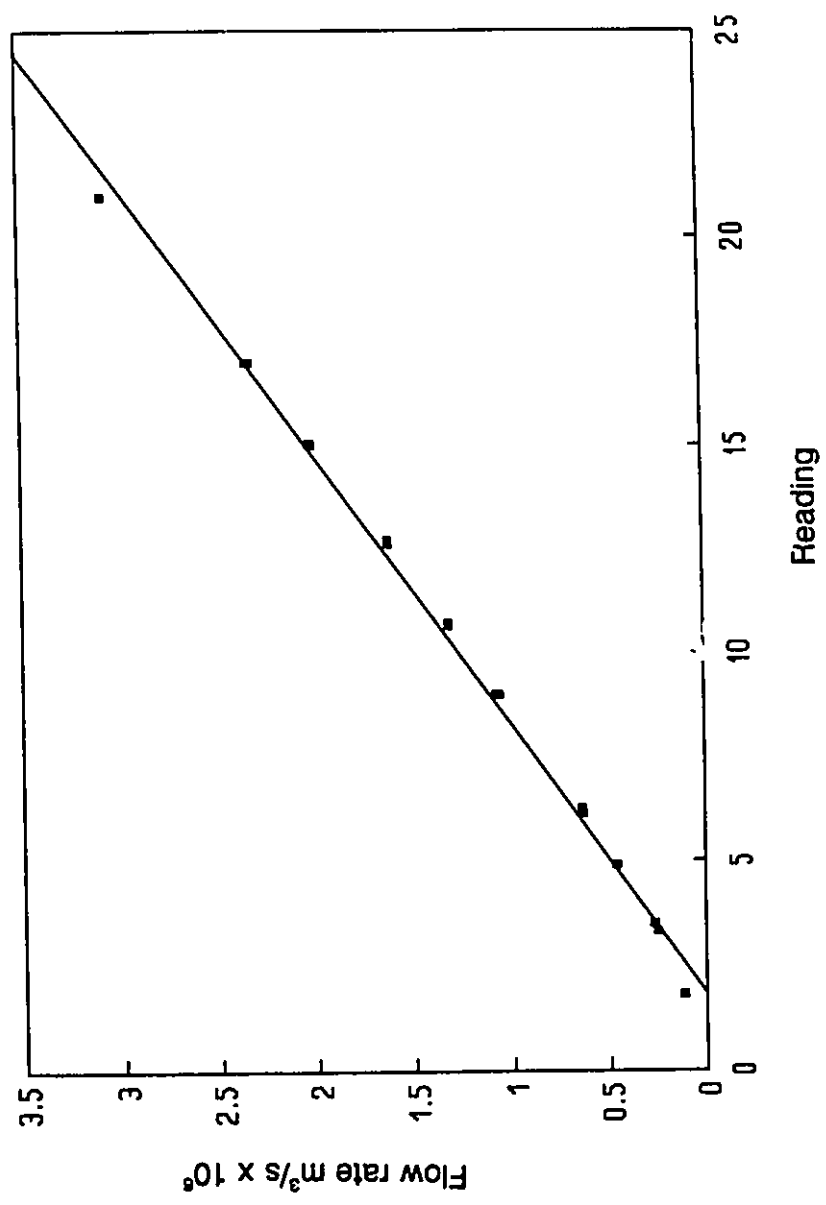


Figure B.1 Calibration Curve Rotameter 1

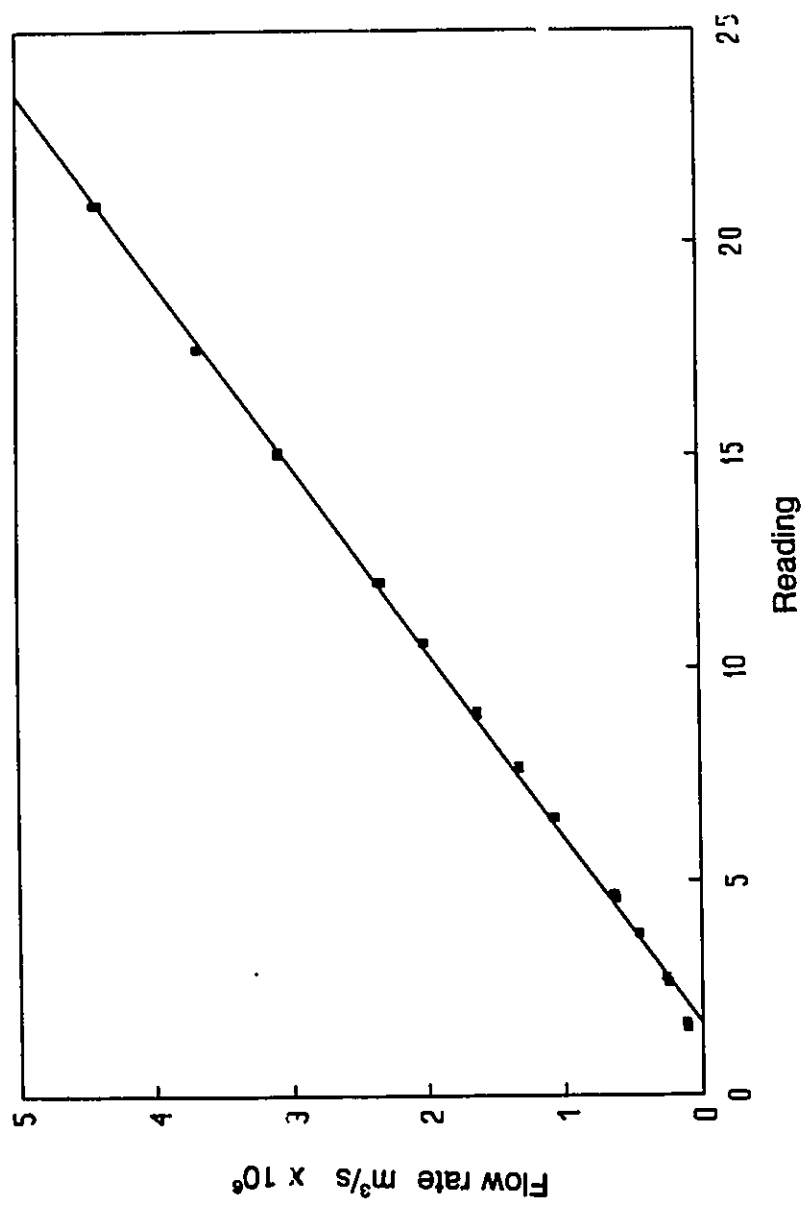


Figure B.2 Calibration Curve Rotameter 2

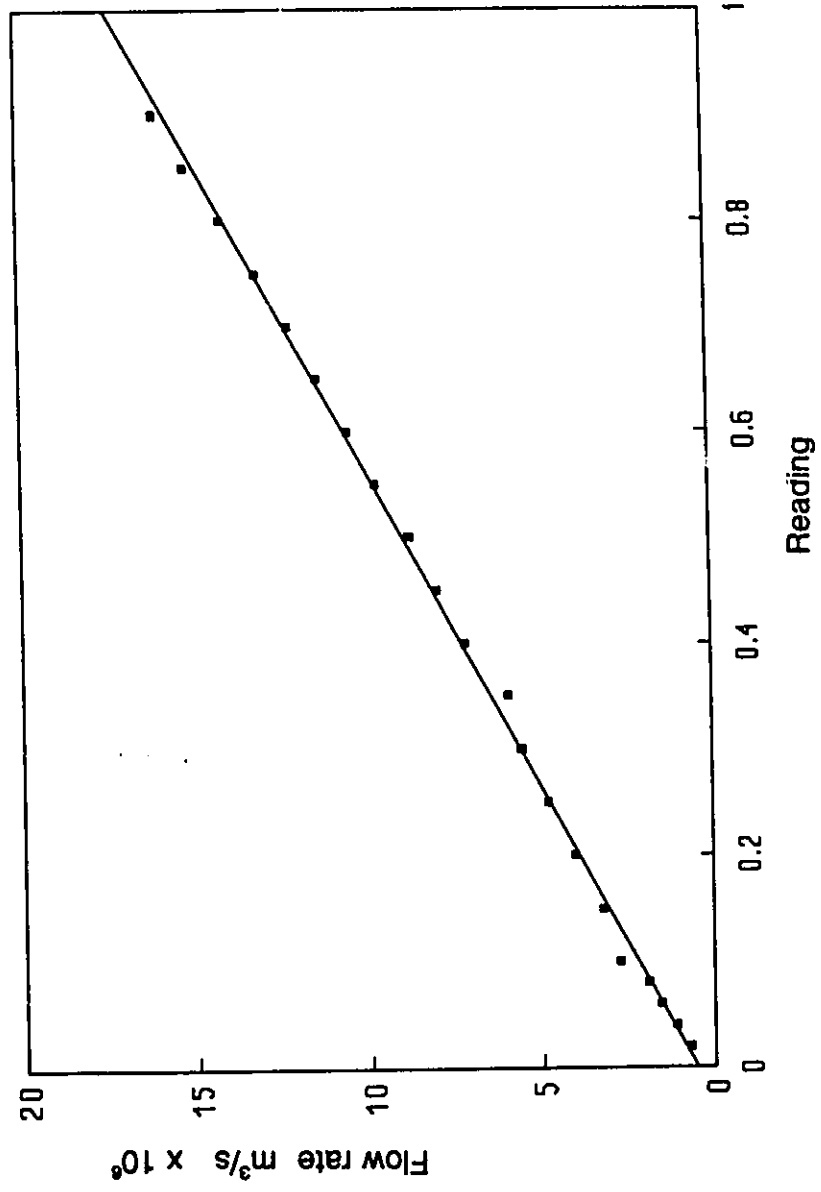


Figure B.3 Calibration Curve Rotameter 3

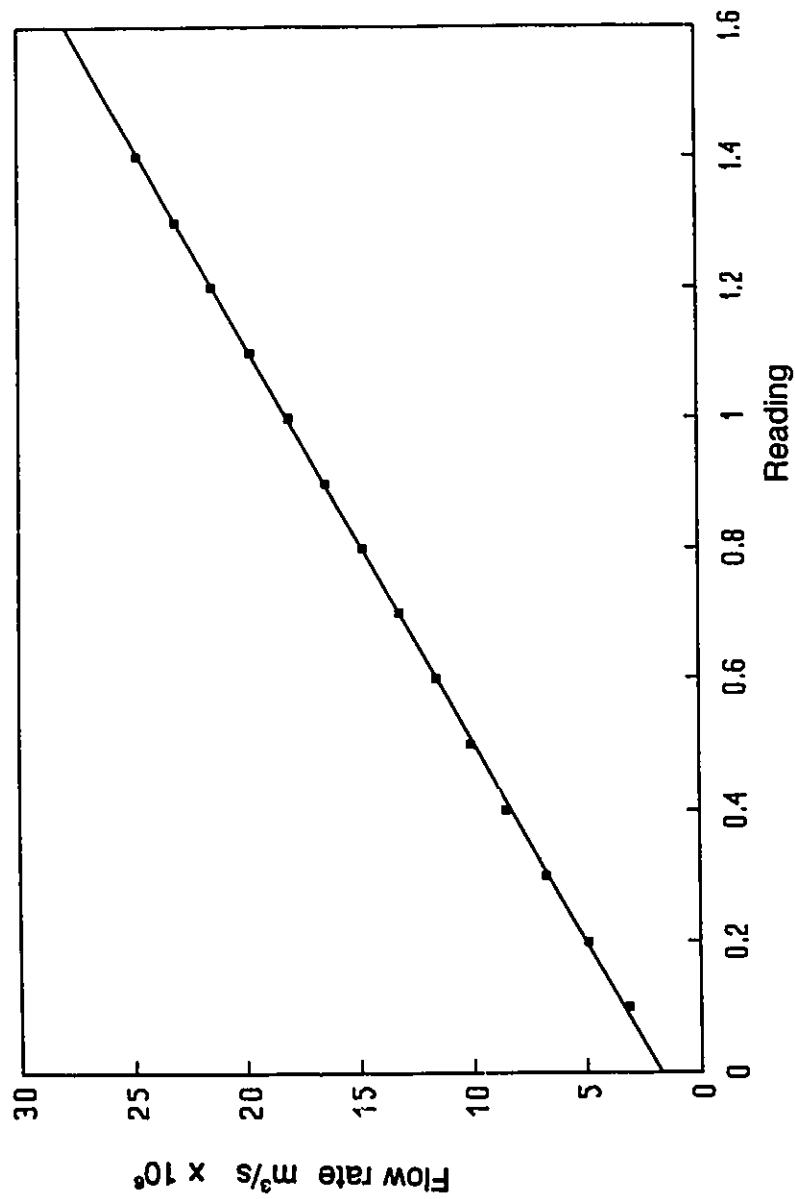


Figure B.4 Calibration Curve Rotameter 4

**APPENDIX D**  
**EXPERIMENTAL DATA**

Diode 1  
Forward Flow

Average Temp. = 21°C

Flow Rate $10^{-6} \text{ m}^3/\text{s}$	Pressure Drop Across Diode Pa.
0.94	17.06
1.12	19.62
1.37	26.44
1.65	32.42
1.91	43.51
2.27	54.58
2.31	57.99
2.38	59.11
2.55	63.98
3.10	89.20
3.51	111.72
3.99	140.17
4.62	177.85
5.19	223.77
5.42	230.26
6.04	299.43
6.88	359.08
7.72	433.44
8.92	553.27
10.90	799.15
11.80	922.24
12.82	1045.45
13.71	1204.66
14.74	1377.52
15.80	1562.15



Diode 1  
Reverse Flow

Average Temp. = 21°C

Flow Rate $10^{-6} \text{ m}^3/\text{s}$	Pressure Drop Across Diode Pa.
1.37	23.04
1.65	33.26
1.73	36.68
1.84	43.50
2.01	51.18
2.27	65.70
2.38	69.94
2.67	93.83
2.75	95.55
3.10	129.67
3.21	140.86
3.62	174.05
3.99	220.07
5.19	401.98
7.10	860.63
7.97	1106.77
8.92	1401.57
9.75	1746.09
11.80	2779.12
12.82	3417.94
13.71	4107.34
14.74	4819.80
15.80	5804.22

Diode 2  
Forward Flow

Average Temp. = 21°C

Flow Rate $10^{-6} \text{ m}^3/\text{s}$	Pressure Drop Across Diode Pa.
3.59	11.49
4.64	15.67
5.60	19.72
7.25	26.44
8.09	31.56
8.94	35.84
9.78	42.65
9.93	47.75
10.60	49.47
11.50	57.15
12.31	63.98
13.22	75.07
14.00	80.14
14.74	90.42
15.70	100.60
16.55	107.51
18.10	127.06
19.73	150.08

Diode 2  
Reverse Flow

Average Temp. = 21°C

Flow Rate $10^{-6} \text{ m}^3/\text{s}$	Pressure Drop Across Diode Pa.
5.02	20.47
5.60	24.74
6.66	37.87
7.25	44.36
8.30	60.97
8.94	73.37
9.93	94.53
10.60	110.04
12.31	154.79
13.22	184.28
14.00	214.71
15.70	276.74
16.55	307.33
18.10	390.76
20.32	513.46
24.11	759.92

Diode 3  
Forward Flow

Average Temp. = 21°C

Flow Rate $10^{-6} \text{ m}^3/\text{s}$	Pressure Drop Across Diode Pa.
9.93	11.93
11.50	16.19
13.22	19.17
14.80	24.91
16.55	29.06
18.10	35.18
19.73	39.71
21.40	49.09
23.00	55.04

Diode 3  
Reverse Flow

Average Temp. = 21°C

Flow Rate $10^{-6} \text{ m}^3/\text{s}$	Pressure Drop Across Diode Pa.
8.29	11.55
9.93	16.59
11.50	23.29
13.22	33.44
14.80	42.33
16.55	54.63
18.10	67.56
19.73	86.07
21.40	102.28
23.00	120.18

**VITA AUCTORIS**

- 1966 Born in Calcutta, India on August 9.
- 1984 Completed Higher Secondary School at Madras Christian College Higher Secondary School, Madras, India in May.
- 1988 Received the Degree of Bachelor of Engineering from Anna University, Madras, India in June.
- 1992 Candidate for the Degree of Master of Applied Science in Mechanical Engineering at University of Windsor, Windsor, Ontario, Canada